Received: 6 October 2023 | Revised: 12 March 2024 | Accepted: 13 March 2024

DOI: 10.1002/ardp.202300575

FULL PAPER

ARCH PHARM DPhG
Archiv der Pharmazie

Novel multifunctional tacrine–donepezil hybrids against Alzheimer's disease: Design synthesis and bioactivity studies

Gülşah Bayraktar[1] | Manuela Bartolini[2] | Maria Laura Bolognesi[2] | Mumin Alper Erdoğan[3] | Güliz Armağan[4] | Ece Bayır[5] | Aylin Şendemir[6] | Donatella Bagetta[7] | Stefano Alcaro[7] | Vildan Alptüzün[1]

[1]Department of Pharmaceutical Chemistry, Faculty of Pharmacy, Ege University, Izmir, Turkey

[2]Department of Pharmacy and Biotechnology, Alma Mater Studiorum—University of Bologna, Bologna, Italy

[3]Department of Physiology, Katip Celebi University School of Medicine, Izmir, Turkey

[4]Department of Biochemistry, Faculty of Pharmacy, Ege University, Izmir, Turkey

[5]Ege University Central Research Test and Analysis Laboratory Application and Research Center (EGE-MATAL), Ege University, Izmir, Turkey

[6]Department of Bioengineering, Faculty of Engineering, Ege University, Izmir, Turkey

[7]Dipartimento di Scienze della Salute, Università degli Studi "Magna Græcia" di Catanzaro, Campus "S. Venuta", Catanzaro, Italy

Correspondence
Vildan Alptüzün, Department of Pharmaceutical Chemistry, Faculty of Pharmacy, Ege University, 35100, Izmir, Turkey.
Email: vildan.alptuzun@ege.edu.tr

Funding information
Ege University Research Foundation; Research Grants from Ege University, Grant/Award Number: 16ECZ023

Abstract

A series of tacrine–donepezil hybrids were synthesized as potential multifunctional anti-Alzheimer's disease (AD) compounds. For this purpose, tacrine and the benzylpiperidine moiety of donepezil were fused with a hydrazone group to achieve a small library of tacrine–donepezil hybrids. In agreement with the design, all compounds showed inhibitory activity toward both acetylcholinesterase (AChE) and butyrylcholinesterase (BChE) with IC_{50} values in the low micromolar range. Kinetic studies on the most potent cholinesterase (ChE) inhibitors within the series showed a mixed-type inhibition mechanism on both enzymes. Also, the docking studies indicated that the compounds inhibit ChEs by dual binding site (DBS) interactions. Notably, tacrine–donepezil hybrids also exhibited significant neuroprotection against H_2O_2-induced cell death in a differentiated human neuroblastoma (SH-SY5Y) cell line at concentrations close to their IC_{50} values on ChEs and showed high to medium blood–brain barrier (BBB) permeability on human cerebral microvascular endothelial cells (HBEC-5i). Besides, the compounds do not cause remarkable toxicity in a human hepatocellular carcinoma cell line (HepG2) and SH-SY5Y cells. Additionally, the compounds were predicted to also have good bioavailability. Among the tested compounds, **H4**, **H16**, **H17**, and **H24** stand out with their biological profile. Taken together, the proposed novel tacrine–donepezil scaffold represents a promising starting point for the development of novel anti-ChE multifunctional agents against AD.

KEYWORDS
AChE inhibition, BBB permeability, BChE inhibition, neuroprotection, tacrine–donepezil hybrid

1 | INTRODUCTION

Alzheimer's disease (AD) is the most common form of dementia worldwide. According to the World Alzheimer's Report in 2018, 50 million people were affected by dementia, and this number is expected to triplicate by the end of 2050.[1,2] As the life expectancy increases, the incidence of the disease expands in parallel.[3] In contrast to its huge impact on the economy of countries, the drug development failure rate in AD is significantly high.[3,4] The lack of distinctive biomarkers to support cognitive tests for a proper and

early diagnosis and the multifactorial nature of AD are considered important factors contributing to this high attrition rate.[5–7]

Most of the approved anti-Alzheimer therapeutics worldwide rely on the so-called "cholinergic hypothesis," which is based on the observation that in AD patients, there is a clear impairment in the cholinergic system in the brain areas that are involved in memory and cognition. In agreement with this hypothesis, a series of anti-cholinesterase agents with different selectivity profiles toward the two cholinesterase (ChE) enzymes, namely, acetylcholinesterase (AChE) and butyrylcholinesterase (BChE), have been approved for the symptomatic treatment of AD.[8]

Other than cholinergic impairment, AD is characterized by well-defined pathological hallmarks, which include amyloid-β (Aβ) peptide aggregation and neurofibrillary tangles formation.[9,10] Aducanumab (Aduhelm™, Biogen), an anti-Aβ monoclonal antibody, was approved by the Food and Drug Administration (FDA) and has become the first disease-modifying therapy.[3] Recently, the humanized immunoglobulin gamma 1 (IgG1) monoclonal antibody lecanemab-irmb (Leqembi™, Eisai-Biogen), which specifically recognizes soluble and insoluble Aβ aggregates, was also granted accelerated approval by the FDA.[11]

Apart from classical hallmarks such as cholinergic impairment, Aβ aggregation, and neurofibrillary tangles formation, AD pathology is also characterized by calcium and biometal dyshomeostasis, enhanced oxidative stress, neuroinflammation, and mitochondrial dysfunction.[9,10,12] Although those pathological features seem to be interconnected, the link between them remains elusive. Therefore, an extensive investigation is in progress.

Concerning oxidative stress, a progressive accumulation of reactive oxygen species (ROS) naturally occurs during brain aging. This is a consequence of the progressive decrease of the antioxidant capacity of the brain, which is paralleled by a higher oxygen consumption. Furthermore, Aβ plaques may act as a ROS reservoir, while increased ROS levels are known to trigger the amyloid cascade. Therefore, antioxidants may also be beneficial to tackle the disease.[9,10,12,13]

Drug discovery approaches for ChE inhibitors have also evolved in the last decades in parallel with the increasing knowledge of the role of those enzymes in AD and their interconnection with other AD players. Indeed, the hydrolysis of the neurotransmitter acetylcholine (ACh) and subsequent termination of the cholinergic transmission has led to a reconsideration of the role of BChE in moderate forms of the disease. Since AChE/BChE ratio significantly decreases with AD progression, due to a progressive loss of cholinergic neurons, BChE is supposed to play an increasing compensatory role as ACh hydrolyzing enzyme.[14–16] In light of this observation, nonselective ChE inhibitors, cholinesterase inhibitors acting at both enzymes or BChE-selective inhibitors might be beneficial in compensating cholinergic impairment in mild-to-moderate forms of AD.[17,18]

Furthermore, AChE may trigger Aβ aggregation by acting as a molecular chaperone, and this noncatalytic function seems to involve the enzyme's peripheral binding site (PAS).[14] This finding has triggered the development of AChE inhibitors acting as dual binding site (DBS) ligands, which are compounds able to simultaneously interact with both PAS and catalytic active site (CAS) with the aim of enhancing the cholinergic transmission and simultaneously inhibit AChE-mediated Aβ aggregation. As a result, these compounds could be more beneficial owing to their interference with amyloidogenic pathways to exert not only symptomatic but also disease-modifying effects.[19,20] Regarding anti-Alzheimer drug discovery, various DBS AChE inhibitors served as initial multitarget-directed ligands (MTDLs).[18,21]

A variety of MTDLs were, indeed, developed keeping in mind the multifactorial nature of the disease and rather palliative clinical effects of the approved small-molecule drugs. –In the scenario, design, synthesis, and bioactivity evaluation of new tacrine-donepezil hybrids were presented here.

1.1 | Design of novel tacrine–donepezil hybrids

Notwithstanding tacrine, the first ChE inhibitor approved by the FDA was withdrawn from the market due to its hepatotoxicity; tacrine scaffold is considered an intriguing pharmacophore in the design of MTDLs endowed with anticholinesterase activities, thanks to its good inhibitory activity toward both AChE and BChE, tolerance to minor structural modifications, relatively easier synthetic protocols and lipophilic nature which eases blood–brain barrier (BBB) penetration. Besides, choosing a simple core such as tacrine may limit issues related to high molecular weight and low solubility.[22] Furthermore, it has been largely shown by several groups that tacrine scaffold can be variously decorated and linked to other pharmacophoric fragments to obtain hybrid molecules that are able to trigger multiple anti-Alzheimer responses such as reduction of ROS levels, inhibition of Aβ aggregation, reduction of Aβ-induced oxidative stress or H_2O_2-induced apoptosis, and inhibition of multiple enzymes involved in AD pathology other than ChEs.[22,23] Tacrine exerts its inhibitory action by binding the CAS of ChEs (with a slight preference for BChE). However, it also shows a lower affinity for AChE's PAS, as shown by X-ray analyses of tacrine homodimers.[19,23]

Donepezil, the first-choice medication in AD management, is an AChE-selective inhibitor that interacts with both of the AChE binding sites. In detail, the indanone moiety interacts with PAS while benzylpiperidine lies along the gorge toward CAS, establishing π–π and cation–π interactions.[24] Owing to the DBS inhibitory mechanism of action, donepezil is also able to prevent, although to a quite limited extent, AChE-induced amyloid aggregation.[25]

In this work, a hydrazone fragment was selected as a connecting fragment to widen the biological profile of the novel tacrine–donepezil hybrids. Indeed, we previously reported the synthesis and characterization of the biological profile of 1,4-dihydropyridine hydrazones and pyridinium hydrazones. Those compounds showed good ChE inhibition as well as inhibitory properties toward Aβ aggregation.[26,27] Hydrazone-bearing compounds were also reported by others to be endowed with antioxidant and neuroprotective properties.[28]

Herein, in the pursuit of novel multifunctional anti-AD agents, we rationally designed and synthesized a small library of tacrine–donepezil

hybrids as ChE inhibitors endowed also with cell protective capacity. To this aim, we selected a tacrine scaffold and the benzylpiperidine moiety of donepezil as core structures and fused them using a hydrazone functional group (Figure 1). The effect of introducing different electron withdrawing or electron-donating groups at different positions of the benzyl ring on the bioactivity was explored to define structure–activity relationships for this new class of hybrids. Besides, a phenethyl derivative was also synthesized to explore the impact of chain length on the activity.

Hence, 26 novel hydrazone-containing tacrine–donepezil hybrids were synthesized, and their activity profile was assessed toward AChE and BChE enzymes. For the most promising hybrids, neuroprotective properties against H_2O_2-induced cell death were evaluated. The hepatotoxic potential of hybrids was also tested against the human hepatocellular carcinoma cell line (HepG2). To get further insights into the mechanism of action in vitro kinetic studies and molecular docking studies were performed. Furthermore, physicochemical properties of the title compounds were calculated. Last but not least, in consideration of the pursued central action, the blood–brain barrier (BBB) permeability of selected hybrids was also evaluated using an in vitro cell-based model.

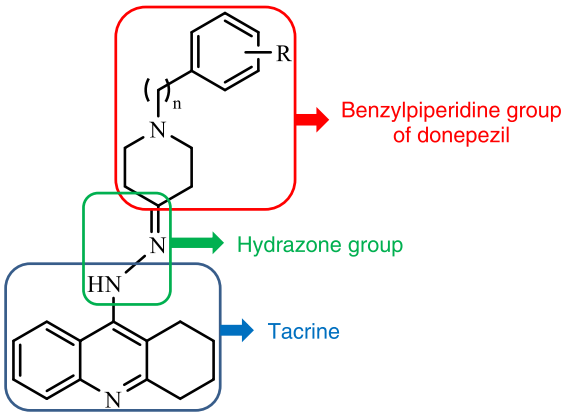

FIGURE 1 Design of the novel tacrine–donepezil hybrids.

2 | RESULTS AND DISCUSSION

2.1 | Chemistry

The synthesis of novel tacrine–donepezil hybrids was realized in four steps, as summarized in Scheme 1.

Anthranilic acid and cyclohexanone were reacted with $POCl_3$ to obtain 9-chloro-1,2,3,4-tetrahydroacridine (**1**).[29] Following the crystallization of crude product from acetone, **1** underwent an aromatic nucleophilic substitution with hydrazine hydrate in n-propanol to give 9-chloro-1,2,3,4-tetrahydroacridine hydrochloride (**2**).[27] The two broad singlets at δ 5.43 pmm and δ 9.72 ppm in the ^{1}H NMR spectra of **2** indicated the hydrazine group introduction to the 1,2,3,4-tetrahydroacridine ring. Additionally, the absence of chlorine isotopic pattern (3:1 relative intensity of ($[M+H]^+/[M+H+2]^+$)) in the mass spectrum of **2** also confirmed the substitution with the hydrazine group.

On the other hand, to obtain various substituted benzylpiperidinone intermediates (**3–28**), substituted benzyl bromides/chlorides were reacted with piperidinone hydrochloride in the presence of K_2CO_3 in acetonitrile:water (1:1) then the oily residue was purified by column chromatography.[30] The structures of substituted benzylpiperidinone intermediates were confirmed by mass spectra and IR spectra/melting points, and the data were in accordance with the literature.[30] Regarding mass spectra, the presence of chlorine (**7**, **15**, **22**, **28**) and bromine (**8**, **16**, **23**) was confirmed by the observed

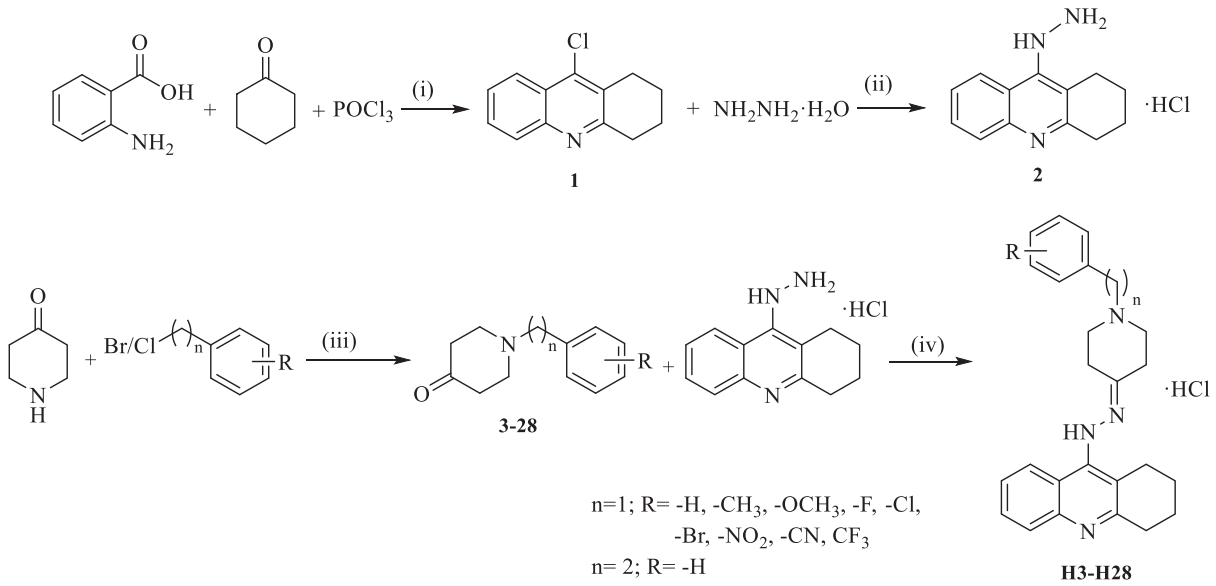

SCHEME 1 Synthesis of the novel tacrine–donepezil hybrids. Reagents and conditions: (i) reflux, 2 h; (ii) *n*-propanol, reflux, 25 h; (iii) K_2CO_3, acetonitrile/water (1:1), reflux, 4 h; (iv) ethanol, rt, 8–12 h.

isotopic pattern with the relative intensity of 3:1 ($[M+H]^+/[M+H+2]^+$) and 1:1 ($[M+H]^+/[M+H+2]^+$), respectively. The carbonyl stretching band of ketone was observed between 1712 and 1704 cm^{-1} in the IR spectra.

In the last step, compound **2** and various substituted benzylpiperidinone derivatives (**3–28)** were stirred in ethanol to obtain the final compounds. Intriguingly, oily and unstable products formed for all reactions except for **H17**, **H18**, **H19**, **H24**, and **H25**. Hydrochloride salts were prepared from the unstable oily compounds by the addition of aqueous 2 N HCl to improve stability and solubility.

The identity of final compounds was confirmed by acquiring IR, ^1H NMR, ^{13}C NMR, two-dimensional (2D) NMR, and mass spectroscopic techniques.

The proton signals were observed with the expected splitting patterns, coupling constant at the expected chemical shifts in the ^1H NMR spectra. DEPT 135, COSY, HSQC, and HMBC analyses were performed on **H3** (nonsubstituted derivative) for further characterization as a representative compound; therefore, considering the observed interactions, the signals in ^1H and ^{13}C spectra of **H3** were assigned in the structure in Section 4 (see Supporting Information S2: spectra 5–10).

In ^1H NMR spectra of the title compounds, generally, 18 aliphatic and eight aromatic protons were observed along with the exchangeable protons. On the other hand, piperidine hydrogens were observed in the higher field (δ 2.57–2.87 ppm) for the compounds that have not been treated with HCl for salt formation, namely **H17**, **H18**, **H19**, **H24**, and **H25**. The methylene protons of the benzyl group were detected with a δ 3.66–4.73 ppm chemical shift as singlet peaks. Multiplet splitting patterns were observed for these protons in the *o*-substituted phenyl derivatives due to the steric effects of the substituents. The exchangeable $-N^+H$ protons due to salt formation were seen between *δ* 10.13–10.26, *δ* 14.33–14.70, and *δ* 11.42–12.55 ppm chemical shifts, as broad singlets, except **H4**, **H17**, **H18**, **H19**, and **H25**.

The assessment of the signals and chemical shifts in ^{13}C NMR spectra demonstrated that the aromatic and aliphatic carbons were observed in the expected regions. Regarding DEPT135 spectra of **H3**, the representative compound, the signals observed between *δ* 20.0–58.0 ppm and *δ* 118.5–132.4 ppm indicated nine methylene and seven methine carbons, respectively. The absence of the signals (*δ* 110.8, 115.2, 138.0, 150.1, 151.3, 159.7 ppm) that were observed in ^{13}C NMR spectra confirmed that these signals belong to quaternary carbon atoms. Similar patterns in ^{13}C NMR spectra were observed for other derivatives depending on their substitutions.

The calculated monoisotopic *m/z*, $[M+H]^+$, for tested compounds were in accordance with the experimental values; moreover, the presence of chlorine (**H7**, **H15**, **H22**, **H28**) and bromine (**H8**, **H16**, **H23**) was confirmed by the observed isotopic pattern. Additionally, the observed *m/z* 198 peak was in association with the 9-amino-1,2,3,4-tetrahydroacridine cation.

The purity of the final compounds was determined by elemental analysis, and the analytical results were within ±0.4% of the calculated values.

2.2 | Bioactivity evaluation

2.2.1 | Cholinesterase inhibition

The inhibitory potencies of all final hybrids toward AChE and BChE were evaluated by Ellman's method using AChE from an electric eel, human recombinant AChE, equine BChE and BChE from human serum (Table 1).[31] The tested derivatives showed inhibitory activities, expressed as IC_{50} values, in the micromolar to submicromolar range.

Considering *ee*AChE inhibition, all compounds showed inhibitory potency ranging from 0.105 to 0.718 µM. The comparison of the nonsubstituted derivative to substituted compounds roughly revealed that the introduction of substituents to the phenyl ring increases the inhibitory potency. Substitution on *o*- and *m*- positions of the phenyl group enhanced the inhibitory activity more than *p*- substitution, with the exception of methyl group (**H5**, **H12**, and **H20**). Generally, bromo- and nitro- containing derivatives exhibited the highest activity while the presence of a trifluoromethyl substituent led to the least active compounds in *o*- and *p*- substituted series. The introduction of a second *o*- substitution (**H6**, **H27** and **H7**, **H28**) did not cause any significant change in the activity. Besides, to continue with *o*- position, the isosteric replacement of a hydrogen with a fluorine atom resulted in a higher potency (compare **H6**, **H27** to **H3**). Lastly, an increase in the inhibitory activity in phenethyl derivative (**H4**) in comparison with the benzyl-bearing derivative (**H3**) was observed.

When moving to the inhibition of the human isoform of the enzyme, a slight decrease in the inhibitory activity was observed compared with *ee*AChE. Notwithstanding this lower activity, all compounds inhibited *h*AChE in the low micromolar range (IC_{50}: 0.50–6.10 µM).

Similar to *ee*AChE inhibition, the introduction of substituents to the phenyl ring generally increased the inhibitory activity. However, taking into account the position of substituents, *m*- and *p*- substitutions favored the activity rather than *o-positioned* substitutions. For instance, considering fluorine-containing derivatives, *m*- and *p*-substituted compounds were more potent than the unsubstituted ones, while the *o*-substituted derivatives were less potent. On the other hand, the 2,6-disubstitution of the benzyl ring with a fluorine (**H27**) and a chlorine (**H28**) showed a potency similar to a nonsubstituted derivative (**H3**). Besides, nitro-containing compounds exhibited the highest inhibitory activity in their respective *o*-, *m*-, *p*- substituted series, followed by cyano-bearing derivatives. Regarding the *o*-substituted series, a remarkable decrease in activity was observed when the fluoro and trifluoromethyl groups were introduced. Similarly, compound **H5** (bearing a methyl substitution) exhibited a twofold increased inhibitory activity compared with its bioisoster, **H11** (trifluoromethyl derivative). On the other hand, phenethyl derivative (**H4**) showed a remarkably higher inhibitory potency in comparison with benzyl derivative (**H3**) for both *ee*AChE and *h*AChE with the IC_{50} values of 0.196 and 0.05 µM, respectively. Based on this, it might be speculated that the distance between 1,2,3,4-tetrahydroacridine and phenyl rings plays a role in the interaction with the enzyme gorge.

TABLE 1 IC_{50} values of the final compounds against AChE and BChE enzymes.

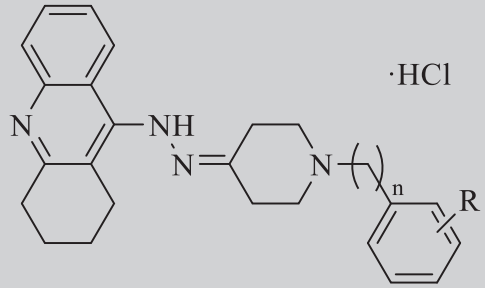

Compound	-R	n	*ee*AChE IC_{50} (μM)	*h*AChE IC_{50} (μM)	*eq*BChE IC_{50} (μM)	*h*BChE IC_{50} (μM)	SI (*h*AChE/*h*BChE)
H3	-H	1	0.24 ± 0.056	2.550 ± 0.530	0.164 ± 0.003	0.318 ± 0.001	8.23
H4	-H	2	0.196 ± 0.008	0.501 ± 0.080	0.079 ± 0.012	0.045 ± 0.029	11.93
H5	2-CH_3	1	0.154 ± 0.006	2.970 ± 0.090	0.103 ± 0.004	0.274 ± 0.003	10.84
H6	2-F	1	0.161 ± 0.005	3.262 ± 0.060	0.063 ± 0.002	0.433 ± 0.019	7.53
H7	2-Cl	1	0.231 ± 0.012	1.710 ± 0.200	0.141 ± 0.005	0.368 ± 0.008	4.65
H8	2-Br	1	0.137 ± 0.004	1.703 ± 0.200	0.098 ± 0.002	0.227 ± 0.012	7.50
H9	2-NO_2	1	0.155 ± 0.006	1.190 ± 0.010	0.035 ± 0.003	0.110 ± 0.003	10.82
H10	2-CN	1	0.239 ± 0.010	1.760 ± 0.130	0.445 ± 0.092	0.138 ± 0.005	12.75
H11	2-CF_3	1	0.274 ±0.015	6.101 ± 0.860	0.075 ± 0.003	0.367 ± 0.020	16.62
H12	3-CH_3	1	0.312 ± 0.011	nd.	0.131 ± 0.007	nd.	nd.
H13	3-OCH_3	1	0.151 ± 0.004	1.690 ± 0.060	0.115 ± 0.007	0.299 ± 0.011	5.65
H14	3-F	1	0.145 ± 0.007	1.682 ± 0.210	0.083 ± 0.013	0.357 ± 0.025	4.71
H15	3-Cl	1	0.108 ± 0.003	2.471 ± 0.150	0.028 ± 0.0003	0.279 ± 0.090	8.86
H16	3-Br	1	0.152 ± 0.004	1.140 ± 0.221	0.071 ± 0.004	0.148 ± 0.030	7.70
H17	3-NO_2	1	0.105 ± 0.006	0.830 ± 0.050	0.127 ± 0.003	0.295 ± 0.013	2.81
H18	3-CN	1	0.211 ± 0.006	1.102 ± 0.040	0.235 ± 0.020	0.466 ± 0.019	2.36
H19	3-CF_3	1	0.263 ± 0.006	1.240 ± 0.280	0.363 ± 0.051	0.679 ± 0.052	1.83
H20	4-CH_3	1	0.220 ± 0.005	2.040 ± 0.130	0.064 ± 0.002	0.278 ± 0.018	7.34
H21	4-F	1	0.288 ± 0.009	1.520 ± 0.120	0.236 ± 0.010	0.325 ± 0.009	4.68
H22	4-Cl	1	0.429 ± 0.015	1.340 ± 0.330	0.108 ± 0.024	0.340 ± 0.011	3.94
H23	4-Br	1	0.227 ± 0.010	3.384 ± 0.610	0.066 ± 0.008	0.402 ± 0.016	8.42
H24	4-NO_2	1	0.239 ± 0.013	0.740 ± 0.070	0.137 ± 0.003	0.275 ± 0.017	2.69
H25	4-CN	1	0.250 ± 0.018	0.930 ± 0.100	0.223 ± 0.008	0.405 ± 0.032	2.30
H26	4-CF_3	1	0.718 ± 0.025	2.102 ± 0.250	0.188 ± 0.008	0.467 ± 0.021	4.50
H27	2,6-diF	1	0.169 ± 0.005	2.160 ± 0.240	0.183 ± 0.004	0.589 ± 0.033	3.67
H28	2,6-diCl	1	0.261 ± 0.006	2.703 ± 0.400	0.099 ± 0.004	0.201 ± 0.008	13.45
Tacrine-HCl	-	-	0.041 ± 0.005	0.320 ± 0.010	0.005 ± 0.0006	0.035 ± 0.005	9.14

Abbreviations: AChE, acetylcholinesterase; BChE, butyrylcholinesterase; nd., not determined.

Concerning the inhibition of *eq*BChE, the compounds inhibited the enzyme with the IC_{50} values differentiating from 0.028 to 0.445 μM. Among the substituents, methyl, chloro, bromo, and nitro favored the activity while cyano disfavored it. Besides, halogen substitution remarkably increased the activity when introduced in the *m*eta position. On the other hand, in line with what was observed for AChE, the phenethyl derivative showed stronger inhibitory potency than the benzyl-bearing compound (**H3**).

Regarding *h*BChE, all compounds inhibited the enzyme in an IC_{50} range of 0.0446–0.679 μM. Similar to what was observed for AChE

inhibition, inhibitory potencies toward the human isoform were lower than those observed with the *eq*BChE. The most active compounds in the *o*- series were derivatives **H9** and **H10**, while compound **H16** was found to be the most potent compound among the *m*-substituted series. Focusing on the derivatives bearing a halogen in the *o*- and *m*- positions, the activity increased in parallel to the substituent's atomic radius. Conversely to what was observed for *o*- and *m*-substituted derivatives, in the *p*-substituted series, the inhibitory potency of halogenated compounds decreased with the increase of the atomic radius. Comparing nitro, cyano, and trifluoromethyl series, the activity increased with the substitution of phenyl ring in the order of *p*-, *m*-, and *o*-positions. On the other hand, fluoro derivatives and trifluoromethyl derivatives showed weaker activity in comparison with the corresponding unsubstituted and methyl-substituted derivatives.

Similar to what was observed with *eq*BChE, lengthening the methylene chain to an ethylene one resulted in a 10-fold increase in the activity. Therefore, phenethyl derivative (**H4**) resulted to be the most active compound toward *h*BChE with an IC_{50} value of 0.045 μM.

The selectivity index (IC_{50}*h*AChE/IC_{50}*h*BChE) of the compounds was calculated to be 1.83–16.62, meaning a slight preference for BChE over AChE, that were in agreement with the tacrine scaffold. Considering that BChE levels increase to compensate for declined AChE levels in mild-to-moderate stages of AD, compounds endowed with BChE inhibitory activity might be beneficial for moderate forms of AD.[15,32]

Taken together all ChE (both *ee*AChE and *h*AChE; *eq*BChE and *h*BChE) activity results, substitution of the benzyl group resulted in improving or maintaining inhibitory activity. Yet, no correlation between the nature of the substituent and activity could not be found. On the other hand, the extension of the chain between the phenyl and piperidine ring from methylene (**H3**) to ethylene (**H4**) notably increased the ChE inhibitory activity.

Many different structures have been designed bearing tacrine–donepezil hybrids since the initial example of this class of compounds by Shao et al.[33–35] It was observed that the introduction of tacrine moiety improves the activity greatly by Shao et al.[33] The literature survey indicated that the ChE inhibitory activity of the tacrine–donepezil hybrids was generally improved or kept compared with the parent drugs.[33–35] Similarly, in our study, the ChE inhibitory activity was retrained. All compounds inhibited both AChE and BChE at low μM concentrations, and the most active derivatives were found to be **H17** (IC_{50}: 0.105 μM, *ee*AChE), **H4** (IC_{50}: 0.50 μM, *h*AChE), **H15** (IC_{50}: 0.028 μM, *eq*BChE), and **H4** (IC_{50}: 0.045 μM, *h*BChE).

AChE and BChE inhibition: Kinetic studies

To gain further insights into the mechanism of inhibition of this new class of hybrids, kinetic studies were performed on the most potent compound, **H4**, against both *h*AChE and *h*BChE. Lineweaver–Burk reciprocal plots (1/rate vs. 1/[substrate]) showed an increase in both slope (decreased *Vmax*) and intercepts (higher K_m) with the increase of the inhibitor concentration (Figures 2 and 3). This trend indicated that **H4** is able to bind to both the free and acetylated form of the enzyme. This behavior is likely associated with the ability of **H4** to bind both the CAS and the PAS of AChE. Similarly, enzyme kinetic studies on BChE revealed a mixed-type inhibition. The K_i values were calculated for AChE and BChE as 0.164 and 0.071 μM, respectively (Table 2). On the other hand, the most potent compound, namely **H15** for *ee*AChE and *eq*BChE enzymes, showed similar interaction patterns (Supporting Information S2: Figures S52, S53, Table S3).

2.2.2 | Neuroprotection assay

In consideration of ChE inhibitory activities and design strategy of tacrine–donepezil hybrids, 9 compounds, namely **H4**, **H6**, **H9**, **H15**,

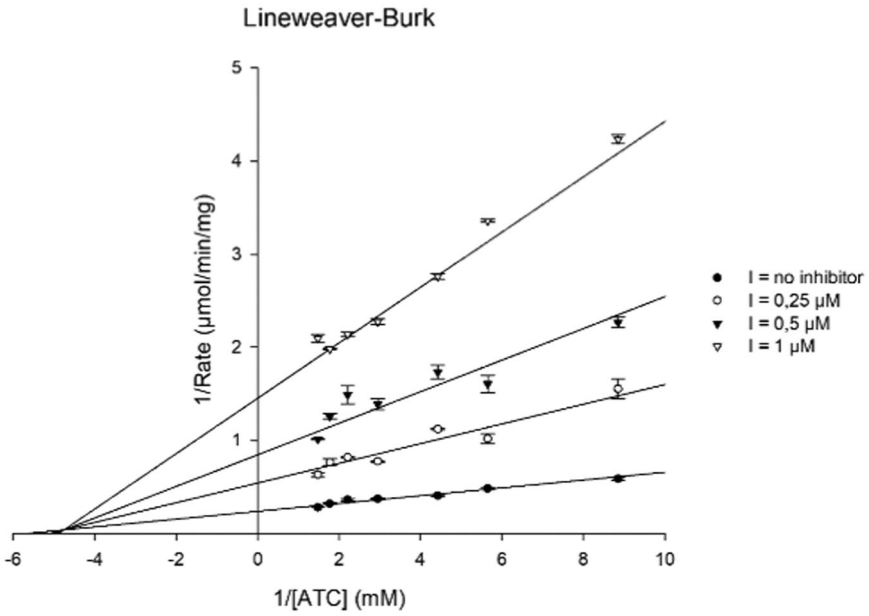

FIGURE 2 Kinetic study on the *h*AChE inhibition of **H4**. Lineweaver–Burk reciprocal plots of 1/*V* versus 1/[ATC].

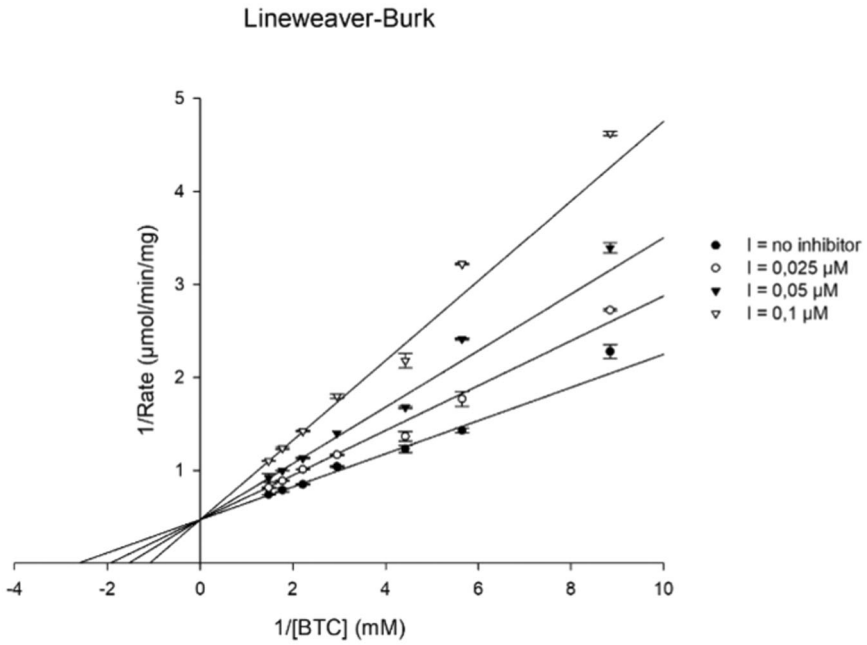

FIGURE 3 Kinetic study on the *h*BChE inhibition of **H4**. Lineweaver–Burk reciprocal plots of 1/V versus 1/[BTC].

TABLE 2 *h*AChE and *h*BChE K_i, V_{max}, and K_m values of **H4**.

	R^2	K_i (µM)	V_{max}	K_m
*h*AChE	0.985	0.164	4.20	0.175
*h*BChE	0.987	0.071	2.10	0.380

Abbreviations: AChE, acetylcholinesterase; BChE, butyrylcholinesterase.

H16, **H17**, **H20**, **H23**, and **H24**, were selected as prototypes of the scaffold and were evaluated for cytotoxic effects and neuroprotective potency against H_2O_2-induced cell death on differentiated human neuroblastoma (SH-SY5Y) cell line. All selected compounds were assayed at 0.1, 1.0, and 10 µM concentrations that are also in the range of their ChE inhibitory potencies. Meanwhile, the hepatotoxic potential of the compounds was tested. None of the tested compounds exhibited any significant cytotoxicity on SH-SY5Y and HepG2 cells up to 10 µM concentration (cell viability: 95.7%–87.2%, Figure 4a and 91.2%–81.4%, Figure 4c), which is fairly above their ChE inhibitory potency.

On the basis of these promising results, the same set of compounds was tested for neuroprotection activity toward H_2O_2-induced cell death using the same cell line. Pretreatment of SH-SY5Y cells with compounds **H4**, **H6**, **H9**, **H15**, **H16**, **H17**, **H20**, **H23**, and **H24** significantly prevented cell death caused by exposure to H_2O_2 as shown in Figure 4b. Noteworthy, all compounds showed similar protective activity to reference compounds resveratrol (5 and 10 µM) and curcumin (50 and 100 µM) at significantly lower concentrations (0.1–10 µM) (Figure 4b, Supporting Information S2: Figure S54). The neuroprotective activity spanned a close range with cell viability percentages comprised between 38.3% and 57.6% (vs. 22.7% cell viability at cells treated with H_2O_2). This may indicate that the neuroprotective effects of the compounds occur in a nondose-dependent manner at tested compound concentrations. The most potent hybrid was compound **H16** which exhibited good neuroprotective effects at concentrations close to its IC_{50} values on ChE, that is, 1.14 and 0.148 µM toward *h*AChE and hBChE. Indeed, cell viability recovered by 30.19% and 34.945% when **H16** was assayed at 0.1 and 1 µM, respectively.

Taken together, the designed tacrine-donepezil scaffold showed a significant neuroprotective potency against H_2O_2-induced cell death at concentrations close to ChE inhibitory potencies.

2.2.3 | In vitro BBB permeability

BBB permeability of the prototype compounds **H6**, **H15**, **H20**, and tacrine were evaluated using human cerebral microvascular endothelial cells (HBEC-5i). Apparent permeability (P_{aap}) values of **H6** (0.1 mM), **H15** (0.1 mM), **H20** (0.1 mM), and tacrine (0.1 and 0.5 mM) were found to be 6.9×10^{-6}, 4.7×10^{-6}, 7.2×10^{-5}, 7.6×10^{-5}, 2.32×10^{-5} cm/s, respectively (Figure 5). Therefore, **H20** and reference compound tacrine possess high permeability, and **H6** and **H15** might be classified as medium BBB permeable compounds. Cell-based investigations confirmed in silico predictions for BBB permeability.

2.3 | Molecular modeling studies

2.3.1 | In silico prediction of the ADME profile

The theoretical pharmacokinetic properties of all derivatives were predicted using the QikProp tool (Supporting Information S2: Table S1). The predicted CNS activity of the compounds was found

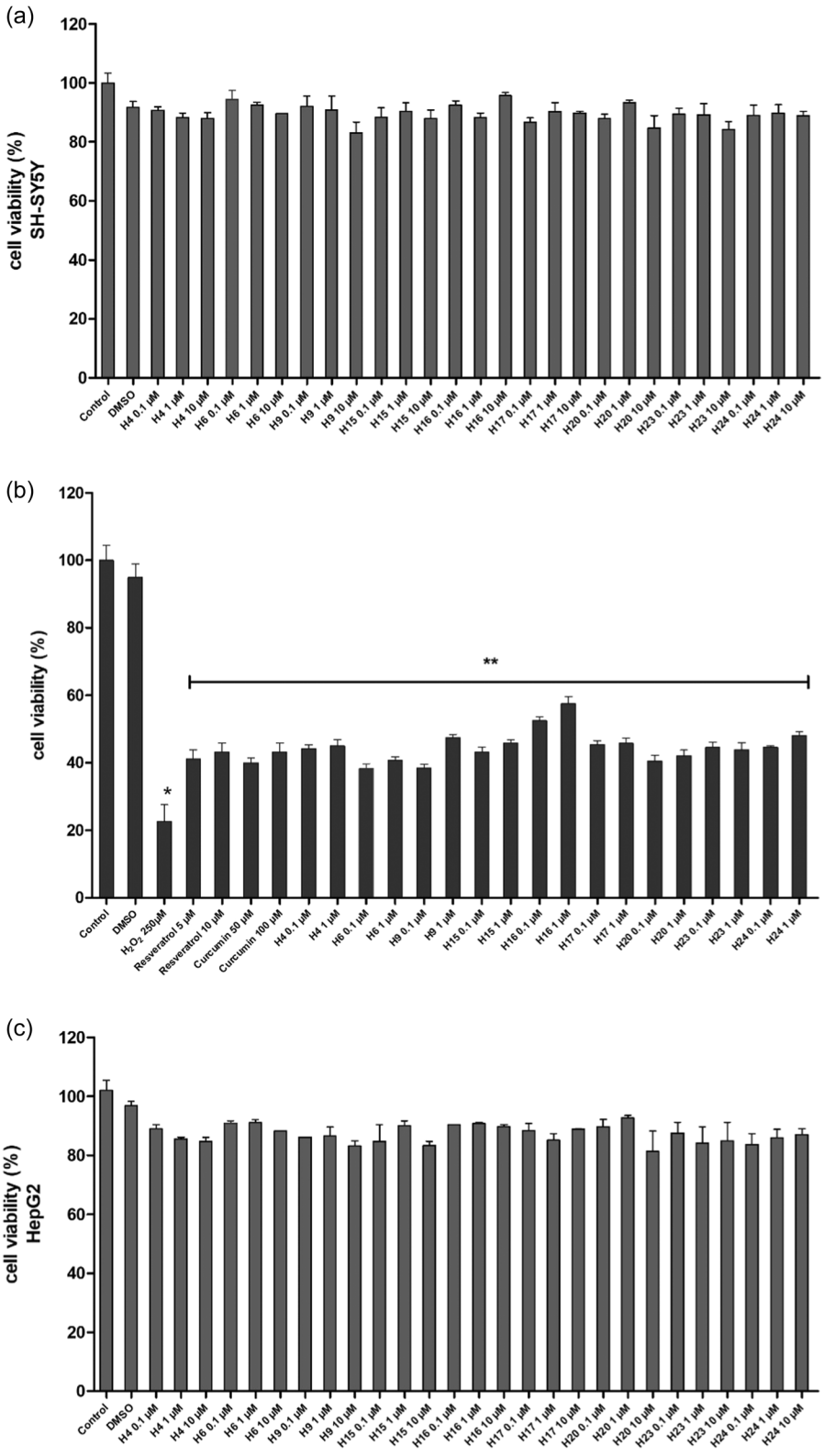

FIGURE 4 (a) Cell viability assay of different concentrations (0.1–10 µM) of compounds on human neuroblastoma cell lines. (b) Percentages of cell viability after exposure to compounds against H_2O_2-treated cells. All values are means ± SDs ($n = 4–6$). *$p < 0.05$ significant difference from untreated and DMSO-treated cells, **$p < 0.05$ significant difference from H_2O_2-treated cells. (c) Cell viability assay of compounds on human hepatocarcinoma cell line (HepG2). All values are means ± SDs ($n = 4–6$). *$p < 0.05$ significant difference from untreated and DMSO-treated cells, **$p < 0.05$ significant difference from H_2O_2-treated cells.

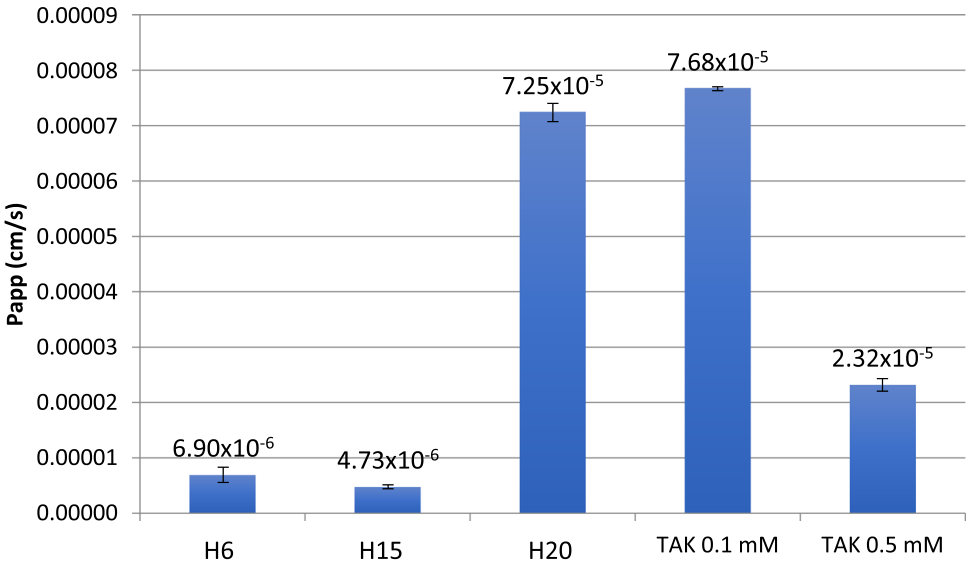

FIGURE 5 Permeability values of **H6** (0.1 mM), **H15** (0.1 mM), **H20** (0.1 mM), and tacrine HCl (TAK 0.1 mM and 0.5 mM) through the obtained BBB model for 60 min.

to be between 0 to +2 (active). Considering the target of the designed compounds, the theoretical predictions were in accordance with the activity of the compounds. Additionally, QPlogBB values ((−0.76) – (+0.64)), an indicator of BBB penetration, were found to be within the recommended range ((−3.0) – (+1.2)) to cross BBB. This was subsequently confirmed by cell-based studies (see the following section). On the other hand, predictions of % oral absorption (92%–100%) indicated compounds should be orally bioavailable. Taken together, the pharmacokinetic predictions by QikProp confirm compliance of the designed scaffold with requirements for oral absorption and BBB permeation as required for their therapeutic application.

2.3.2 | Molecular docking and dynamic simulations

Molecular docking simulations were performed to rationalize the observed experimental outcomes from in vitro investigations with human cholinesterases (*h*ChEs). According to the docking results, although a linear correlation between experimental data and theoretical binding affinity values (Supporting Information S2: Table S2) was not found, all proposed tacrine-donepezil hybrids were able to recognize active sites of both *h*ChEs, establishing interactions with crucial amino acid residues. In particular and in agreement with in vitro kinetic studies, the docking poses obtained for *h*AChE suggested that all ligands were endowed with the capability to interact both with CAS and PAS adopting very similar binding modes (Figure 6 and Supporting Information S2: Figures S1-S25).

Indeed, except for **H13** (Supporting Information S2: Figure S10), **H24** (Supporting Information S2: Figure S21), and **H26** (Supporting Information S2: Figure S23), our derivatives oriented the tetrahydroacridine part toward Trp286 and the variable portion toward the inner side, where most of the CAS residues are located, including Trp86. As a matter of fact, for *h*AChE recognition, we could assume a quite moderate influence of the substituents in agreement with the changes in the inhibitory profiles. Focusing on the most interesting derivative, **H4** (Figure 5), it could bind *h*AChE establishing cation-π/π–π interactions with PAS residues Trp286 and Tyr72 by means of the tetrahydroacridine moiety; piperidine, and phenylethyl groups interacted with CAS residues Tyr341, Tyr337, Trp86. Compared with the binding mode reported for tacrine[36] which mainly interacts with CAS residues Trp86 and His447, **H4** directing the tetrahydroacridine portion to the PAS residues was oriented in an opposite way. Such different orientations could be addressed not just to the **H4** greater steric hindrance with respect to the tacrine structure, but also to the possibility of directing the phenylethyl and piperidine groups similarly to the donepezil.[37] **H4** also displayed favorable binding mode in *h*BChE gorge, establishing cation-π/π–π contacts with Trp82, hydrogen bonds with Asp70, and π–π contacts with Trp231, a key amino acid residue for tacrine binding too.[38]

Analyzing the outcomes from the docking poses of other hybrids on *h*BChE, a low influence of substituents was encountered (Figure 5 and Supporting Information S2: Figures S26-S50). Specifically, derivatives **H5** (Supporting Information S2: Figure S27), **H6** (Supporting Information S2: Figure S28), **H7** (Supporting Information S2: Figure S29), and **H8** (Supporting Information S2: Figure S30) shared almost superimposable binding mode underlining a similar contribution of the methyl, fluorine, chlorine, and bromine atoms at position 2 of the phenyl ring. In particular, docking poses suggested that the tetrahydroacridine moiety establishes cation-π/π–π contacts and hydrogen bonds with the backbone of Trp82 and His438 residues, respectively, while the phenyl ring was involved in π-π interactions with Phe329 and Trp231. A comparable pose was observed for compounds **H12** (Supporting Information S2: Figure S34), **H14**

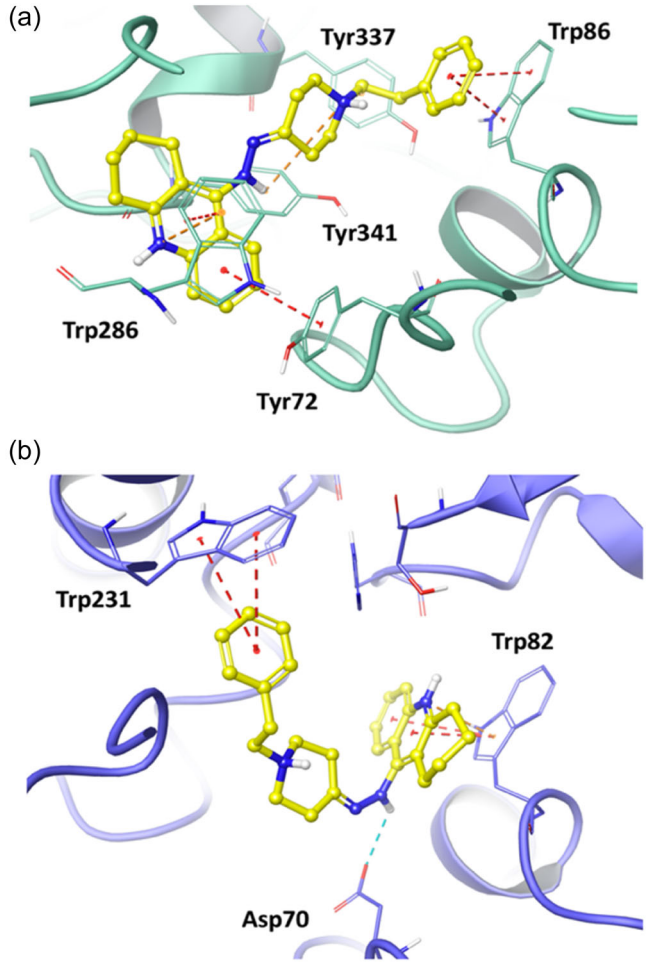

FIGURE 6 Best docking pose of **H4** in the (a) *h*AChE and (b) *h*BChE active sites, represented in green and purple cartoons, respectively. The most relevant interacting residues and the catalytic triad are depicted in the tube; meanwhile, the ligand is shown as a yellow ball and stick representation. π–π interactions, π–cation contacts, and hydrogen bonds are respectively represented in red, orange, and light blue. AChE, acetylcholinesterase; BChE, butyrylcholinesterase.

(Supporting Information S2: Figure S36), and **H27** (Supporting Information S2: Figure S49). This leads to assuming a similar influence of the following: positions 2 and 3 for the methyl group, positions 2-, 3- and 2,6- for the fluorine atom, methyl and fluorine substituents at positions 2 and 3. Conversely, compounds **H13** (Supporting Information S2: Figure S35), **H15** (Supporting Information S2: Figure S37), **H16** (Supporting Information S2: Figure S38), **H17** (Supporting Information S2: Figure S39), and **H20** (Supporting Information S2: Figure S42) showed a different arrangement in the *h*BChE active site. In detail, the tetrahydroacridine moiety interacted with Tyr332 and Asp70. Notwithstanding this different orientation, these two hybrids maintained π–π interactions with Phe329 and/or Trp231. Interestingly the nitro group caused a different effect on ligand configuration depending on its position, however, permitting compound **H9** (Supporting Information S2: Figure S31), **H17** (Supporting Information S2: Figure S39), and **H24** (Supporting Information S2: Figure S46) to execute productive interactions with *h*BChE pivotal residues. In addition, the binding modes of the compound **H24** and **H26** (Supporting Information S2: Figure S48), overlapped, proposing a similar contribution of the nitro and trifluoromethyl groups at position 4. Tetrahydroacridine moiety of both **H24** and **H26** established HB and by π–π interactions with His438 backbone and Trp82, respectively, whereas their charged piperidine nitrogen electrostatically interacted with Asp70. Comparing binding poses of H series (trifluoromethyl analogs), **H11**, **H19**, and **H26** (Supporting Information S2: Figures S33 and S41), equivalent interactions could be detected only for the tetrahydroacridine portion. Concerning derivatives bearing a cyano group, the presence of a cyano group at position 3 (**H18**) (Supporting Information S2: Figure S40) and 4 (**H25**) (Supporting Information S2: Figure S47) produced a similar pose characterized by the formation of a hydrogen bond with His438 backbone and cation-π/π–π contacts with Trp82. On the other hand, when the cyano group was at position 2 (**H10**, Supporting Information S2: Figure S32), the binding mode changed and resulted closer to those observed for compounds **H13** (Supporting Information S2: Figure S35), **H20** (Supporting Information S2: Figure S42), **H15** (Supporting Information S2: Figure S37), **H16** (Supporting Information S2: Figure S38), and **H17** (Supporting Information S2: Figure S39) than to that observed for the other cyano analogs. Compound **H21** (Supporting Information S2: Figure S43), **H22** (Supporting Information S2: Figure S44), and **H23** (Supporting Information S2: Figure S45) bearing halogen atoms at position 4 showed similar binding modes with the tetrahydroacridine fragment establishing a hydrogen bond with the His438 side chain and the piperidine nitrogen interacting with Ty332 and Asp70. Such binding pose was also shared by the not substituted compound **H3** (Supporting Information S2: Figure S26). However, it must be underlined that **H3** could also interact with Trp231 and Phe239. Regarding the 2,6 halogen disubstituted compounds **H27** (Supporting Information S2: Figure S49) and **H28** (Supporting Information S2: Figure S50), they only shared interactions involving the tetrahydroacridine fragment. Then, based on experimental data, the attention was refocused on compound **H4**, and with the aim of deeply evaluating the molecular interactions and their stability with both *h*ChEs, the docking complexes were submitted to 250 ns of molecular dynamics (MD) simulations. As reported in Supporting Information S2: Figure S51, the interactions most stable in the *h*AChE active site were cation-π with Tyr341 and Trp286, confirming the capability of our most promising compound to stably recognize both CAS and PAS sites. Regarding *h*BChE, MD simulations demonstrated the stability of cation-π/π–π contacts with Trp82 and the opportunity to perform additional interactions with Asp70 and Glu197 that characterized the great part of the MD trajectory time.

In conclusion, the molecular modeling computations performed to elucidate the influence of substituents on the benzyl group did not suggest major changes in terms of binding modes. Thus, theoretical studies were concentrated on the compound endowed with the best biological activity, denoting that **H4** is a promising template for developing multifunctional tacrine-donepezil hybrids since it could recognize significant active site residues in both targets.

3 | CONCLUSION

In this study, a series of novel tacrine–donepezil hybrids were designed and synthesized as MTDL compounds acting as ChE inhibitors and endowed with neuroprotective effects.

All compounds exhibited AChE and BChE inhibitory activity at low or submicromolar levels. In general, the substitution on the phenyl ring positively affected inhibitory activity on both enzymes, but no clear SARs on the effect of the position of the substituent on ChE activity could be drawn. In addition, elongation of the linker connecting 1,2,3,4-tetrahydroacridine and phenyl rings improved the inhibitory activity of both enzymes. In vitro and in silico investigations on the mode of inhibition/interaction indicated a mixed-type inhibition for both enzymes and especially in the case of AChE, the compounds can interact with DBSs. Furthermore, studies on neurotoxicity and neuroprotection showed that those hybrids were not significantly neurotoxic and could exert remarkable neuroprotective effects against H_2O_2-induced cell death. Besides, the tested compounds were found to be noncytotoxic on HepG2 cells. In addition, in vitro BBB permeability assay showed that the tested compounds also had a good permeability. Finally, in silico ADME predictions confirmed that tacrine–donepezil hybrids show good bioavailability. Among the title compounds, **H4**, **H16**, **H17**, and **H24** stand out with their promising biological profile.

Although the hybrid molecules are not superior to tacrine and donepezil regarding AChE activity, these hybrids having ChE inhibitory effect at low micromolar levels provide a neuroprotective effect on SH-SY5Y cells and do not cause toxicity on HepG2 cells at similar concentrations to their ChE inhibitory activity. Hence, this hybrid skeleton could be promising for further study to combat AD.

4 | EXPERIMENTAL

4.1 | Chemistry

4.1.1 | General

Regents and solvents were commercially available materials of reagent grade and were purchased from Alfa Aesar, TCI Chemicals, Sigma-Aldrich, VWR, or Merck. Melting points were determined by using a capillary melting point apparatus (Barnstead Electrothermal IA 900). Analytical thin layer chromatography (TLC) was run on Merck silica gel plates (Kieselgel 60 F254), and detection was performed by using a UV lamp (254 nm). Merck silica gel 60 was used as a stationary phase for column chromatography. The FT-IR spectra of the compounds were acquired by attenuated total reflectance (ATR) (PerkinElmer Spectrum 100 FT-IR, Shelton). Nuclear magnetic resonance (NMR) spectra (400 MHz for ^{1}H NMR and 100 MHz for ^{13}C NMR) were recorded in deuterated DMSO on an AS400 Mercury Plus NMR Varian (Varian Inc.) and a Bruker AV 400 instrument (Bruker Biopsin). Chemical shifts were measured in parts per million (δ). Coupling constants (*J*) are reported in hertz (Hz). Splitting patterns were designated as follows: s (singlet); d (doublet); t (triplet); ddd (doublet doublet doublet); td (triplet doublet); bs (broad singlet), and m (multiplet). Liquid chromatography–mass spectrometry (LC/MS) analyses were performed on a Thermo MSQ Plus/DSQ II mass spectrometer equipped with an electrospray (ESI) ion source in positive mode. Elemental analyses were performed on a Leco TruSpec Micro CHNS (Leco, St. Joseph), and obtained values were within ±0.4% of the theoretical values.

The InChI codes of the investigated compounds, together with some biological activity data, are provided as Supporting Information.

4.1.2 | General procedure for the synthesis of 9-chloro-1,2,3,4-tetrahydroacridine (1)

A volume of 3 mL $POCl_3$ was added into a mixture of 740 mg anthranilic acid (5.39 mmol) and 0.54 mL cyclohexanone (5.17 mmol) in an ice bath. The reaction mixture was refluxed for 3 h. After cooling down, the reaction media was neutralized with a saturated K_2CO_3 solution. The aqueous phase was extracted with ethyl acetate (3 × 50 mL). Collected ethyl acetate was washed with brine, dried over Na_2SO_4, and evaporated under reduced pressure. The crude product was crystallized from acetone.[29] Yellow crystal; 45% yield; mp 67°C (crys. from acetone)[39]; IR (ATR) ν_{maks}: 3050, 2937, 2869, 1612, 1578, 1533, 1481, 766, 752 cm^{-1}; ^{1}H NMR (400 MHz, DMSO-d_6): δ 1.91–1.95 (m, 4H), 2.94–3.08 (m, 4H), 7.60 (ddd, *J* = 8.2/6.9/1.2 Hz, 1H), 7.71 (ddd, *J* = 8.4/6.9/1.4 Hz, 1H), 7.93 (d, *J* = 8,4 Hz, 1H), 8.14 (d, *J*= 8,4 Hz, 1H) ppm; MS (ESI, MeOH) *m/z*: 218.38 ([M+H]$^+$, 100%), 220.33 ([M+H+2]$^+$, 32%).

4.1.3 | General procedure for the synthesis of 9-hydrazino-1,2,3,4-tetrahydroacridine hydrochloride (2)

9-Chloro-1,2,3,4-tetrahydroacridine (2.17 g, 10 mmol) and 0.66 mL hydrazine hydrate (10 mmol) were refluxed for 25 h in *n*-propanol. The precipitate was filtered and used without further purification.[27] Yellow crystal; 79% yield; mp 290°C[40]; IR (ATR) ν_{maks}: 3169, 3045, 2985, 2838, 1630, 1591, 1520, 1474, 1450, 1430, 761, 677 cm^{-1}; ^{1}H NMR (400 MHz, DMSO-d_6): δ 1.81 (d, *J* = 5.3 Hz, 4H), 2.51–2.56 (m, 2H), 2.92 (t, *J* = 5.3 Hz, 2H), 5.43 (bs, 2H), 7.44 (ddd, *J* = 8.5/6.80/1.4 Hz, 1H), 7.78 (ddd, *J* = 8.4/6.8/1.2 Hz, 1H), 7.84 (dd, *J* = 8,5/1.1 Hz, 1H), 9.50–9.57 (m, 1H), 9.72 (bs, 1H), 13.44 (bs, 1H) ppm; MS (ESI, MeOH) *m/z*: 214.40 ([M+H]$^+$, 100%), 215.33 ([M+H+1]$^+$, 11%).

4.1.4 | General procedure for the synthesis of 1-(substitutedbenzyl)-4-piperidinone derivatives (3–28)

Various substituted-benzyl bromide/chloride (5.2 mmol) and K_2CO_3 (8.4 mmol) were added into the solution of 648 mg 4-piperidinone monohydrate hydrochloride (4.2 mmol) in acetonitrile/water (1:1). The mixture was refluxed for 4 h, extracted with CH_2Cl_2 then washed with

brine and evaporated under reduced pressure. The oily residue was purified by column chromatography (ethyl acetate/*n*-hexane 7:3).[30]

1-Benzylpiperidin-4-one (**3**): Compound **3** was provided commercially.

1-Phenethylpiperidin-4-one (**4**): Beige solid; 45% yield; mp 57°C [41]; MS (ESI, MeOH) *m/z*: 105.26 ($[C_8H_9]^+$, 100%), 204.39 ($[M+H+]^+$, 31%), 205.33 ($[M+H+1]^+$, 4%).

1-(2-Methylbenzyl)piperidin-4-one (**5**): Pale yellow oil; 70% yield; MS (ESI, MeOH) *m/z*: 118.29 ($[C_8H_8N]^+$, 100%), 204.35 ($[M+H+]^+$, 62%), 205.33 ($[M+H+1]^+$, 6%).

1-(2-Fluorobenzyl)piperidin-4-one (**6**): Pale yellow oil; 71% yield; MS (ESI, MeOH) *m/z*: 109.24 ($[C_7H_6F]^+$, 100%), 150.31 ($[C_9H_9FN]^+$, 86%), 208.34 ($[M+H+]^+$, 43%), 209.33 ($[M+H+1]^+$, 7%).

1-(2-Chlorobenzyl)piperidin-4-one (**7**): Pale yellow oil; 51% yield; MS (ESI, MeOH) *m/z*: 166.19 ($[C_9H_9ClN]^+$, 100%), 224.35 ($[M+H]^+$, 66%), 226.33 ($[M+H+2]^+$, 23%).

1-(2-Bromobenzyl)piperidin-4-one (**8**): Beige crystal; 65% yield; mp 71°C; MS (ESI, MeOH) *m/z*: 210.21 ($[C_9H_{10}BrN]^+$, 100%), 212.21 ($[M+H]^+$, 32%), 270.28 ($[M+H+2]^+$, 31%).

1-(2-Nitrobenzyl)piperidin-4-one (**9**): Light orange crystal; 67% yield; mp 75°C; MS (ESI, MeOH) *m/z*: 136.26 ($[C_7H_6NO_2]^+$, 100%), 235.32 ($[M+H+]^+$, 24%), 236.30 ($[M+H+1]^+$, 5%).

1-(2-Cyanobenzyl)piperidin-4-one (**10**): White crystal; 80% yield; mp 65 °C; MS (ESI, MeOH) *m/z*: 157.28 ($[C_{10}H_9N_2]^+$, 100%), 215.35 ($[M+H]^+$, 10%), 216.31 ($[M+H+1]^+$, 2%).

1-[2-(Trifluoromethyl)benzyl]piperidin-4-one (**11**): Yellow crystal; 76% yield; mp 72 °C; MS (ESI, MeOH) *m/z*: 200.32 ($[C_{10}H_9F_3N]^+$, 100%), 258.34 ($[M+H]^+$, 34%), 259.34 ($[M+H+1]^+$, 4%).

1-(3-Methylbenzyl)piperidin-4-one (**12**): Pale yellow oil; 69% yield; MS (ESI, MeOH) *m/z*: 105.28 ($[C_8H_9]^+$, 100%), 204.41 ($[M+H+]^+$, 49%), 205.33 ($[M+H+1]^+$, 6%).

1-(3-Methoxybenzyl)piperidin-4-one (**13**): Pale yellow oil; 72% yield; MS (ESI, MeOH) *m/z*: 162.30 ($[C_{10}H_{12}NO]^+$, 100%), 220.34 ($[M+H+]^+$, 36%), 221.33 ($[M+H+1]^+$, 6%).

1-(3-Fluorobenzyl)piperidin-4-one (**14**): Pale yellow oil; 73% yield; MS (ESI, MeOH) *m/z*: 150.33 ($[C_9H_9FN]^+$, 75%), 208.34 ($[M+H+]^+$, 100%), 209.33 ($[M+H+1]^+$, 20%).

1-(3-Chlorobenzyl)piperidin-4-one (**15**): Pale yellow oil; 75% yield; MS (ESI, MeOH) *m/z*: 166.15 ($[C_9H_9ClN]^+$, 100%), 224.26 ($[M+H]^+$, 55%), 226.33 ($[M+H+2]^+$, 16%).

1-(3-Bromobenzyl)piperidin-4-one (**16**): Pale yellow oil; 51% yield; MS (ESI, MeOH) *m/z*: 268.40 ($[M+H]^+$, 59%), 270.40 ($[M+H+2]^+$, 44%), 300.41 ($[M+H+CH_3OH]^+$, 100%), 302.41 ($[M+H+CH_3OH+2]^+$, 96%).

1-(3-Nitrobenzyl)piperidin-4-one (**17**): Orange crystal; 79% yield; mp 78 °C MS (ESI, MeOH) *m/z*: 177.37 ($[C_9H_9N_2O_2]^+$, 100%), 235.35 ($[M+H+]^+$, 51%), 236.31 ($[M+H+1]^+$, 6%).

1-(3-Cyanobenzyl)piperidin-4-one (**18**): Yellow crystal; 73% yield; mp 53 °C; MS (ESI, MeOH) *m/z*: 157.28 ($[C_{10}H_9N_2]^+$, 100%), 215.35 ($[M+H]^+$, 63%), 216.31 ($[M+H+1]^+$, 8%).

1-[3-(Trifluoromethyl)benzyl]piperidin-4-one (**19**): Yellow oil; 75% yield; MS (ESI, MeOH) *m/z*: 200.32 ($[C_{10}H_9F_3N]^+$, 95%), 258.34 ($[M+H]^+$, 100%), 259.34 ($[M+H+1]^+$, 10%).

1-(4-Methylbenzyl)piperidin-4-one (**20**): Pale yellow oil; 78% yield; MS (ESI, MeOH) *m/z*: 105.28 ($[C_8H_9]^+$, 100%), 204.41 ($[M+H+]^+$, 13%), 205.33 ($[M+H+1]^+$, 4%).

1-(4-Fluorobenzyl)piperidin-4-one (**21**): Pale yellow oil; 60% yield; MS (ESI, MeOH) *m/z*: 109.23 ($[C_7H_6F]^+$, 100%), 208.34 ($[M+H+]^+$, 53%), 209.33 ($[M+H+1]^+$, 13%).

1-(4-Chlorobenzyl)piperidin-4-one (**22**): Pale yellow oil; 85% yield; MS (ESI, MeOH) *m/z*: 125.25 ($[C_7H_6Cl]^+$, 100%), 224.32 ($[M+H]^+$, 51%), 226.33 ($[M+H+2]^+$, 16%).

1-(4-Bromobenzyl)piperidin-4-one (**23**): Yellow crystal; 80% yield; mp 64 °C(lit); MS (ESI, MeOH) *m/z*: 268.40 ($[M+H]^+$, 7%), 270.39 ($[M+H+2]^+$, 7%), 300.37 ($[M+H+CH_3OH]^+$, 99%), 302.41 ($[M+H+CH_3OH+2]^+$, 99%).

1-(4-Nitrobenzyl)piperidin-4-one (**24**): Beige crystal; 60% yield; mp 106 °C; MS (ESI, MeOH) *m/z*: 235.41 ($[M+H+]^+$, 64%), 236.33 ($[M+H+1]^+$, 10%), 267.47 ($[M+H+CH_3OH]^+$, 100%).

1-(4-Cyanobenzyl)piperidin-4-one (**25**): Pale yellow oil; 52% yield; MS (ESI, MeOH) *m/z*: 157.24 ($[C_{10}H_9N_2]^+$, 100%), 215.35 ($[M+H]^+$, 57%), 216.33 ($[M+H+1]^+$, 8%).

1-[4-(Trifluoromethyl)benzyl]piperidin-4-one (**26**): Pale yellow oil; 67% yield; MS (ESI, MeOH) *m/z*: 200.28 ($[C_{10}H_9F_3N]^+$, 100%), 258.34 ($[M+H]^+$, 47%), 259.34 ($[M+H+1]^+$, 6%).

1-(2,6-Difluorobenzyl)piperidin-4-one (**27**): Beige crystal; 62% yield; mp 90 °C; MS (ESI, MeOH) *m/z*: 168.24 ($[C_9H_8F_2N]^+$, 100%), 226.34 ($[M+H]^+$, 27%), 227.33 ($[M+H+1]^+$, 3%).

1-(2,6-Dichlorobenzyl)piperidin-4-one (**28**): White crystal; 68% yield; mp 82 °C; MS (ESI, MeOH) *m/z*: 200.26 ($[C_9H_8Cl_2N]^+$, 100%), 258.28 ($[M+H]^+$, 46%), 260.33 ($[M+H+2]^+$, 26%), 262.31 ($[M+H+4]^+$, 5%).

4.1.5 | General procedure for the synthesis of 9-[2-(1-substitutedbenzylpiperidin-4-ylidene)hydrazinyl]-1,2,3,4-tetrahydroacridine hydrochloride derivatives (**H3–H28**)

A mixture of 249 mg 9-hydrazinyl-1,2,3,4-tetrahydroacridine (1 mmol) and 1-(substitutedbenzyl)-4-piperidinone (1 mmol) in ethanol was stirred for 8–12 h. In the case of **H17**, **H18**, **H19**, **H24**, and **H25**, the formed precipitate was filtered, then washed with cool ethanol, and crystallized from isopropanol.[27] Due to difficulties in the purification of the compounds, the title products except **H17**, **H18**, **H19**, **H24**, and **H25** were isolated in their 3 mole HCl salt forms. To isolate the compounds in their 3 mole HCl salt forms, the reactions were treated with 2 N HCl after the evaporation of the ethanol under vacuum. The formed precipitate was filtered and crystallized using an isopropanol/methanol (1:1) mixture.

9-[2-(1-Benzylpiperidin-4-ylidene)hydrazinyl]-1,2,3,4-tetrahydroacridine trihydrochloride (**H3**): Yellow crystal; 64% yield; mp 246°C (crys. from isopropanol); IR (ATR) ν_{maks}: 2947, 2682, 2549, 1631, 1583, 1519, 1474, 1428, 1407, 752, 699 cm^{-1}; ^1H NMR (400 MHz, DMSO-d_6): δ 1.78-1.88 (m, 4H, H-2, H-3), 2.72–3.31 (m, 10H, H-1, H-4, H-2'/H-6', H-3', H-5'), 3.49–3.60 (m, 2H, H-2'/H-6'), 4.34–4.50 (m, 2H, NH-$\underline{CH_2}$-phenyl),

7.43–7.49 (m, 3H, H-3", H-4", H-5"), 7.50 (t, *J*=7.9 Hz, 1H, H-7), 7.68–7.74 (m, 2H, H-2", H-6"), 7.85 (t, *J* = 7.7 Hz, 1H, H-6), 8.08 (d, *J* = 8.5 Hz, 1H, H-8), 9.06 (d, *J* = 8.8 Hz, 1H, H-5), 10.18 (bs, 1H, NH), 12.21 (bs, 1H, NH), 14.67 (bs, 1H, NH) ppm; ^{13}C NMR (100 MHz, DMSO-d_6): δ 20.2 (C-2/C-3), 21.2 (C-2/C-3), 23.5 (C-1/C-4), 25.0 (C-3'/C-5'), 27.9 (C-1/C-4), 30.6 (C-3'/C-5'), 49.49 (C-2'/C-6'), 50.1 (C-2'/C-6'), 58.2 (NH-$\underline{CH_2}$-phenyl), 110.8 (C-9a), 115.2 (C-8a), 118.7 (C-8), 125.17 (C-7), 127.9 (C-5), 20.2 (C-2/C-3), 128.7 (2 C, C-3"/C-4"/C-5"), 129.4 (C-3"/C-4"/C-5"), 129.8 (C-1"), 131.4 (2 C, C-2", C-6"), 132.59 (C-6), 138.0 (C-10a), 150.1 (C-9), 151.3 (C-4a), 159.7 (C-4') ppm; MS (ESI, MeOH) *m/z*: 184.35 ([$C_{13}H_{13}N$]$^+$, 47%), 197.35 ([$C_{13}H_{11}N_2$]$^+$, 59%), 385.38 ([M+H]$^+$, 100%), 386.39 ([M+H+1]$^+$, 23%); elemental analysis, calcd. for $C_{25}H_{28}N_4$·3 HCl·0.5 C_3H_7OH: C, 60.75; H, 6.73; N, 10.69; found: C, 60.78; H, 6.89; N, 10.96.

9-[2-(1-Phenethylpiperidin-4-ylidene)hydrazinyl]-1,2,3,4-tetrahydroacridine trihydrochloride (**H4**): Yellow crystal; 23% yield; mp 245°C (crys. from isopropanol); IR (ATR) ν_{maks}: 2938, 2874, 2652, 2513, 2465, 1633, 1585, 1513, 1474, 1436, 1405, 758, 702 cm^{-1}; ^{1}H NMR (400 MHz, DMSO-d_6): δ 1.77–1.89 (m, 4H), 2.78–3.32 (m, 14H), 3.72–3.86 (m, 2H), 7.22–7.41 (m, 5H), 7.54 (t, *J* = 8.3 Hz, 1H), 7.86 (t, *J* = 7.5 Hz, 1H), 8.09 (d, *J* = 8.6 Hz, 1H), 9.09 (d, *J* = 8.8 Hz, 1H), 10.21 (bs, 1H), 12.05 (bs, 1H) ppm; ^{13}C NMR (100 MHz, DMSO-d_6): δ 20.3, 21.3, 23.5, 25.2, 28.0, 29.5, 30.7, 49.8, 50.7, 55.9, 110.9, 115.2, 118.7, 125.2, 126.8, 128.0, 128.6 (2 C), 128.7, 132.6, 137.1, 138.0, 150.1, 151.4, 159.5 ppm; MS (ESI, MeOH) *m/z*: 197.35 ([$C_{13}H_{11}N_2$]$^+$, 62%), 399.49 ([M+H]$^+$, 100%), 400.41 ([M+H+1]$^+$, 15%); elemental analysis, calcd. for $C_{26}H_{30}N_4$·3 HCl·C_3H_7OH: C, 61.32; H, 7.28; N, 9.86; found: C, 61.64; H, 7.11; N, 9.82.

9-{2-[1-(2-Methylbenzyl)piperidin-4-ylidene]hydrazinyl}-1,2,3,4-tetrahydroacridine trihydrochloride (**H5**): Yellow crystal; 78% yield; mp 242°C (crys. from isopropanol); IR (ATR) ν_{maks}: 3045, 2941, 2860, 2695, 2636, 2569, 1633, 1588, 1517, 1472, 1458, 1410, 756, 742, 676 cm^{-1}; ^{1}H NMR (400 MHz, DMSO-d_6): δ 1.80–1.89 (m, 4H), 2.47 (s, 3H), 2.73–3.32 (m, 10H), 3.55–3.64 (m, 2H), 4.36–4.45 (m, 2H, NH-$\underline{CH_2}$-phenyl), 7.25–7.37 (m, 3H), 7.54 t, *J* = 7.9 Hz, 1H), 7.77 (d, *J* = 7.5 Hz, 1H), 7.86 (t, *J* = 7.8 Hz, 1H), 8.05 (d, *J* = 8.5 Hz, 1H), 9.09 (d, *J* = 8.8 Hz, 1H), 10.17 (bs, 1H), 11.61 (bs, 1H), 14.52 (bs, 1H) ppm; ^{13}C NMR (100 MHz, DMSO-d_6): δ 19.7, 20.3, 21.3, 23.5, 25.5, 28.0, 30.8, 49.9, 50.6, 55.9, 110.9, 115.3, 118.8, 125.3, 126.2, 128.0, 129.6 (2 C), 130.9, 132.4, 132.7, 138.1, 138.7, 150.2, 151.4, 160.0 ppm; MS (ESI, MeOH) *m/z*: 399.49 ([M+H]$^+$, 100%), 400.41 ([M+H+1]$^+$, 18%); elemental analysis, calcd. for $C_{26}H_{30}N_4$·3 HCl·0.05 C_3H_7OH: C, 61.47; H, 6.59; N, 10.97; found: C, 61.62; H, 6.25; N, 11.09.

9-{2-[1-(2-Fluorobenzyl)piperidin-4-ylidene]hydrazinyl}-1,2,3,4-tetrahydroacridine trihydrochloride (**H6**): Yellow crystal; 60% yield; mp 132°C (crys. from isopropanol); IR (ATR) ν_{maks}: 2917, 2849, 2695, 2576, 1632, 1585, 1521, 1494, 1456, 1403, 767, 677 cm^{-1}; ^{1}H NMR (400 MHz, DMSO-d_6): δ 1.78–1.87 (m, 4H), 2.73–3.23 (m, 10H), 3.55–3.66 (m, 2H), 4.45 (s, 2H), 7.29–7.37 (m, 2H), 7.49–7.58 (m, 2H), 7.84 (ddd, *J* = 8.3/7.1/1.1 Hz, 1H), 7.90 (td, *J* = 7.7/1.3, 1H), 8.08 (d, *J* = 7.9 Hz, 1H), 9.06 (d, *J* = 8.3 Hz, 1H), 10.16 (bs, 1H), 12.23 (bs, 1H), 14.69 (bs, 1H) ppm; ^{13}C NMR (100 MHz, DMSO-d_6): δ 20.3, 21.2, 23.5, 25.2, 28.0, 30.8, 49.5, 50.4, 51.3, 110.9, 115.2, 115.7, 115.9, 118.7, 124.9, 125.2, 128.0, 132.6, 134.3, 138.0, 150.1, 151.34, 159.5, 160.0, 162.42 ppm; MS (ESI, MeOH) *m/z*: 403.39 ([M+H]$^+$, 100%), 404.40 ([M+H+1]$^+$, 25%); elemental analysis, calcd. for $C_{25}H_{27}FN_4$·3 HCl·1.5 H_2O: C, 55.72; H, 6.17; N, 10.40; found: C, 55.54; H, 5.87; N, 10.73.

9-{2-[1-(2-Chlorobenzyl)piperidin-4-ylidene]hydrazinyl}-1,2,3,4-tetrahydroacridine trihydrochloride (**H7**): Yellow crystal; 66% yield; mp 158°C (crys. from isopropanol); IR (ATR) ν_{maks}: 3041, 2847, 2776, 2695, 2576, 1631, 1584, 1522, 1473, 1445, 1403, 861, 767, 677 cm^{-1}; ^{1}H NMR (400 MHz, DMSO-d_6): δ 1.79–1.90 (m, 4H), 2.71–3.30 (m, 10H), 3.54–3.68 (m, 2H), 4.54 (s, 2H), 7.45–7.61 (m, 4H), 7.86 (ddd, *J* = 8.3/6.9/1.0 Hz, 1H), 8.05–8.11 (m, 2H), 9.08 (d, *J* = 8.6 Hz, 1H), 10.17 (bs, 1H), 12.19 (bs, 1H), 14.66 (bs, 1H) ppm; ^{13}C NMR (100 MHz, DMSO-d_6): δ 20.3, 21.2, 23.5, 25.2, 27.9, 30.8, 49.8, 50.7, 55.2, 110.9, 115.2, 118.7, 125.2, 127.7, 128.0, 129.8 (2 C), 131.5, 132.6, 134.2, 134.7, 138.1, 150.2, 151.4, 159.6 ppm; MS (ESI, MeOH) *m/z*: 198.30 ([$C_{13}H_{12}N_2$]$^+$, 67%), 419.33 ([M+H]$^+$, 100%), 421.37 ([M+H+2]$^+$, 37%); elemental analysis, calcd. for $C_{25}H_{27}ClN_4$·3 HCl·H_2O: C, 54.96; H, 5.90; N, 10.25; found: C, 55.03; H, 5.62; N, 10.16.

9-{2-[1-(2-Bromobenzyl)piperidin-4-ylidene]hydrazinyl}-1,2,3,4-tetrahydroacridine trihydrochloride (**H8**): Yellow crystal; 69% yield; mp 213°C (crys. from isopropanol); IR (ATR) ν_{maks}: 2941, 2856, 2625, 2525, 2416, 1633, 2587, 1516, 1473, 1437, 1409, 756, 676 cm^{-1}; ^{1}H NMR (400 MHz, DMSO-d_6): δ 1.77–1.89 (m,4H), 2.73–3.29 (m, 8H), 3.52–3.66 (m, 4H), 4.55 (s, 2H), 7.41 (t, *J* = 7.7, 1H), 7.49–7.58 (m, 2H), 7.75 (d, *J* = 8.0 Hz, 1H), 7.86 (t, *J* = 7.7 Hz, 1H), 8.07 (d, *J* = 8.5 Hz, 1H), 8.14 (d, *J* = 7.4 Hz, 1H) 9.08 (d, *J* = 8.8 Hz, 1H) 10.16 (bs, 1H), 12.12 (bs, 1H), 14.60 (bs, 1H) ppm; ^{13}C NMR (100 MHz, DMSO-d_6): δ 20.3, 21.3, 23.5, 25.5, 28.0, 30.9, 49.9, 50.8, 57.8, 110.9, 115.2, 118.7, 125.2, 125.4, 128.5, 128.3, 131.7, 132.7, 133.2 (2 C), 134.0, 138.1, 150.2, 151.4, 159.7 ppm; MS (ESI, MeOH) *m/z*: 197.36 ([$C_{13}H_{11}N_2$]$^+$, 100%), 463.21 ([M+H]$^+$, 50%), 465.23 ([M+H+2]$^+$, 51%); elemental analysis, calcd. for $C_{25}H_{27}BrN_4$·3 HCl·0.25 H_2O: C, 52.01; H, 5.33; N, 9.71; found: C, 51.79; H, 5.46; N, 9.33.

9-{2-[1-(2-Nitrobenzyl)piperidin-4-ylidene]hydrazinyl}-1,2,3,4-tetrahydroacridine trihydrochloride (**H9**): Orange crystal; 45% yield; mp 193°C (crys. from isopropanol); IR (ATR) ν_{maks}: 3071, 2951, 2722, 1643, 1589, 1530, 1479, 1442, 1406, 1339, 866, 763,679 cm^{-1}; ^{1}H NMR (400 MHz, DMSO-d_6): δ 1.78–1.89 (m, 4H), 2.76–3.39 (m, 10H), 3.60–3.72 (m, 2H), 4.73 (s, 2H), 7.59 (ddd, *J* = 9.6/6.7/1.0 Hz, 1H), 7.78 (td, *J* = 8.4/1.2 Hz, 1H), 7.83–7.92 (m, 2H), 8.08 (d, *J* = 8,1 Hz, 1H), 8.17–8.24 (m, 2H), 9.08 (d, *J* = 8.7 Hz, 1H) 10.22 (bs, 1H), 11.75 (bs, 1H), 14.63 (bs, 1H) ppm; ^{13}C NMR (100 MHz, DMSO-d_6): δ 20.3, 21.3, 23.6, 25.6, 28.0, 30.7, 50.6, 51.5, 55.4, 110.9, 115.3, 118.8, 125.2, 125.4, 128.0, 128.1, 131.3, 132.7, 134.2, 134.3, 138.1, 149.2, 150.2, 151.4, 159.7 ppm; MS (ESI, MeOH) *m/z*: 197.35 ([$C_{13}H_{11}N_2$]$^+$, 89%), 430.47 ([M+H]$^+$, 100%), 431.40 ([M+H+1]$^+$, 25%); elemental analysis, calcd. for $C_{25}H_{27}N_5O_2$·3 HCl·1.5 H_2O: C, 53.06; H, 5.88; N, 12.38; found: C, 52.84; H, 6.24; N, 12.19.

9-{2-[1-(2-Cyanobenzyl)piperidin-4-ylidene]hydrazinyl}-1,2,3,4-tetrahydroacridine trihydrochloride (**H10**): Yellow crystal; 41% yield; mp 195°C (crys. from isopropanol); IR (ATR) ν_{maks}: 2941, 2889, 2780,

2710, 2625, 2230, 1629, 1585, 1520, 1469, 1448, 1403, 776 cm^{-1}; ^1H NMR (400 MHz, DMSO-d_6): δ 1.77–1.91 (m, 4H), 2.73–3.22 (m, 10H), 3.57–3.69 (m, 2H), 4.48–4.63 (s, 2H), 7.55 (t, *J* = 7.8 Hz, 1H), 7.68 (t, *J* = 7.7 Hz, 1H), 7.83–7.90 (m, 2H), 7.98 (d, *J* = 7.5 Hz, 1H), 8.04 (d, *J* = 8.5 Hz, 1H), 9.09 (d, *J* = 8.8 Hz, 1H), 10.14 (bs, 1H), 12.43 (bs, 1H), 14.49 (bs, 1H) ppm; ^{13}C NMR (100 MHz, DMSO-d_6): δ 20.3, 21.2, 23.5, 25.3, 27.9, 30.8, 50.0, 50.9, 56.5, 110.9, 113.7, 115.2, 117.3, 118.7, 125.2, 128.0, 130.4, 132.6, 133.0 (2 C), 133.5, 133.6, 138.1, 150.2, 151.4, 159.6 ppm; MS (ESI, MeOH) *m/z*: 410.39 ([M+H]$^+$, 100%), 411.38 ([M+H+1]$^+$, 24%); elemental analysis, calcd. for $C_{26}H_{27}N_5$·3 HCl·1.5 H_2O: C, 57.20; H, 6.09; N, 12.38; found: C, 57.60; H, 6.09; N, 12.82.

9-(2-{1-[2-(Trifluoromethyl)benzyl]piperidin-4-ylidene}hydrazinyl)-1,2,3,4-tetrahydroacridine trihydrochloride (**H11**): Yellow crystal; 80% yield; mp 230°C (crys. from isopropanol:methanol); IR (ATR) ν_{maks}: 3013, 2940, 2868, 2699, 2650, 2544, 1634, 1587, 1520, 1474, 1443, 1409, 1310, 1164, 1115, 777, 759, 677 cm^{-1}; ^1H NMR (400 MHz, DMSO-d_6): δ 1.79–1.88 (m, 4H), 2.71–3.33 (m, 10H), 3.52–3.65 (m, 2H), 4.54 (s, 2H), 7.55 (t, *J* = 7.9 Hz, 1H), 7.69 (t, *J* = 7.6 Hz, 1H), 7.81–7.90(m, 3H), 8.07 (d, *J* = 8.5 Hz, 1H), 8.14 (d, *J* = 7.4 Hz, 1H) 9.09 (d, *J* = 8.8 Hz, 1H) 10.16 (bs, 1H), 12.23 (bs, 1H), 14.58 (bs, 1H) ppm; ^{13}C NMR (100 MHz, DMSO-d_6): δ 20.3, 21.3, 23.5, 25.5, 28.0, 30.9, 50.4, 51.3, 55.0, 62.0, 110.9, 115.3, 118.8, 125.2, 126.4 (3 C), 128.0, 130.0, 132.7, 133.1 (2 C), 138.1, 150.2, 151.4, 173.6 ppm; MS (ESI, MeOH) *m/z*: 198.35 ([$C_{13}H_{12}N_2$]$^+$, 56%), 453.49 ([M+H]$^+$, 100%), 454.47 ([M+H+1]$^+$, 26%); elemental analysis, calcd. for $C_{26}H_{27}F_3N_4$·3 HCl·0.1 C_3H_5OH: C, 55.62; H, 5.47; N, 9.87; found: C, 55.34; H, 5.83; N, 9.60.

9-{2-[1-(3-Methylbenzyl)piperidin-4-ylidene]hydrazinyl}-1,2,3,4-tetrahydroacridine trihydrochloride (**H12**): Yellow crystal; 40% yield; mp 195°C (crys. from isopropanol); IR (ATR) ν_{maks}: 2929, 2860, 2772, 2699, 2650, 2569, 1633, 1586, 1518, 1473, 1441, 1406, 776, 698 cm^{-1}; ^1H NMR (400 MHz, DMSO-d_6): δ 1.79-1.90 (m, 4H), 2.33 (s, 3H), 2.70–3.30 (m, 10H), 3.51–3.62 (m, 2H), 4.29–4.44 (m, 2H), 7.21 (d, *J* = 7.6 Hz, 1H), 7.35 (t, *J* = 7.7 Hz, 1H), 7.47–7.57 (m, 3H), 7.86 (t, *J* = 7.7 Hz, 1H), 8.05 (d, *J* = 8.1 Hz, 1H), 9.06 (d, *J* = 8.8 Hz, 1H), 10.16 (bs, 1H), 11.99 (bs, 1H), 14.55 (bs, 1H) ppm; ^{13}C NMR (100 MHz, DMSO-d_6): δ 20.3, 21.0, 21.2, 23.5, 25.0, 28.0, 30.7, 49.5, 50.2, 58.3, 110.9, 115.2, 118.7, 125.3, 128.0, 128.5 (3 C), 128.7, 130.1, 132.0, 132.7, 138.0, 150.2, 151.4, 159.8 ppm; MS (ESI, MeOH) *m/z*: 399.47 ([M+H]$^+$, 100%), 400.41 ([M+H+1]$^+$, 18%); elemental analysis, calcd. for $C_{26}H_{30}N_4$·3 HCl: C, 61.47; H, 6.55; N, 11.03; found: C, 61.88; H, 6.15; N, 11.07.

9-{2-[1-(3-Methoxybenzyl)piperidin-4-ylidene]hydrazinyl}-1,2,3,4-tetrahydroacridine trihydrochloride (**H13**): Yellow crystal; 28% yield; mp 205°C (crys. from isopropanol); IR (ATR) ν_{maks}: 2938, 2835, 2664, 2558, 2423, 1633, 1586, 1515, 1470, 1438, 1406, 1251, 1034, 754, 695 cm^{-1}; ^1H NMR (400 MHz, DMSO-d_6): δ 1.78–1.89 (m, 4H), 2.73–3.29 (m, 10H), 3.50–3.60 (m, 2H), 3.80 (s, 3H), 4.30–4.46 (m, 2H), 7.02 (dd, *J* = 8.1/2.1 Hz, 1H), 7.21 (d, *J* = 7.4 Hz, 1H), 7.36 (t, *J* = 7.9 Hz, 1H), 7.43 (s, 1H), 7.52 (t, *J* = 7.5 Hz, 1H), 7.85 (t, *J* = 7.6 Hz, 1H), 8.01 (d, *J* = 8.4 Hz, 1H), 9.06 (d, *J* = 8.7 Hz, 1H), 10.17 (bs, 1H), 12.18 (bs, 1H), 14.64 (bs, 1H) ppm; ^{13}C NMR (100 MHz, DMSO-d_6): δ 20.2, 21.2, 23.4, 25.0, 28.0, 30.6, 49.5, 50.2, 55.2, 58.2, 110.9, 115.3, 116.7 (2 C), 118.8, 123.3, 125.2, 128.0, 129.8, 129.9, 132.7, 138.0, 150.2, 151.4, 159.4, 160.0 ppm; MS (ESI, MeOH) *m/z*: 197.35 ([$C_{13}H_{11}N_2$]$^+$, 66%), 415.46 ([M+H]$^+$, 100%), 416.39 ([M+H+1]$^+$, 17%); elemental analysis, calcd. for $C_{26}H_{30}N_4O$·3 HCl: C, 59.60; H, 6.35; N, 10.69; found: C, 59.98; H, 6.02; N, 11.04.

9-{2-[1-(3-Fluorobenzyl)piperidin-4-ylidene]hydrazinyl}-1,2,3,4-tetrahydroacridine trihydrochloride (**H14**): Yellow crystal; 63% yield; mp 219°C (crys. from isopropanol); IR (ATR) ν_{maks}: 3052, 2940, 2863, 2689, 2557, 2500, 1633, 1586, 1516, 1490, 1471, 1408, 781, 751, 690 cm^{-1}; ^1H NMR (400 MHz, DMSO-d_6): δ 1.77–1.89 (m, 4H), 2.69–3.31 (m, 10H), 3.51–3.62 (m, 2H), 4.36–4.53 (m, 2H), 7.27–7.35 (m, 1H), 7.59–7.67 (m, 3H), 7.66 (d, *J* = 9 Hz, 1H), 7.85 (ddd, *J* = 8.3/6.9/1.1 Hz, 1H), 8.07 (d, *J* = 8.3 Hz, 1H), 9.06 (d, *J* = 8.7 Hz, 1H), 10.17 (bs, 1H), 12.31 (bs, 1H), 14.62 (bs, 1H) ppm; ^{13}C NMR (100 MHz, DMSO-d_6): δ 20.2, 21.2, 23.5, 25.0, 27.9, 30.6, 49.6, 50.2, 57.4, 110.9, 115.2, 116.3, 116.5, 118.7, 125.2, 127.6, 127.9, 130.8, 130.9, 132.6, 138.0, 150.1, 151.4, 160.7, 163.1 ppm; MS (ESI, MeOH) *m/z*: 198.35 ([$C_{13}H_{12}N_2$]$^+$, 54%), 403.46 ([M+H]$^+$, 100%), 404.40 ([M+H+1]$^+$, 30%); elemental analysis, calcd. for $C_{25}H_{27}FN_4$·3 HCl: C, 58.66; H, 5.91; N, 10.95; found: C, 59.03; H, 5.66; N, 10.73.

9-{2-[1-(3-Chlorobenzyl)piperidin-4-ylidene]hydrazinyl}-1,2,3,4-tetrahydroacridine trihydrochloride (**H15**): Yellow crystal; 38% yield; mp 225°C (crys. from isopropanol); IR (ATR) ν_{maks}: 2937, 2856, 2660, 2540, 2395, 1633, 1586, 1518, 1474, 1436, 1406, 869, 778, 702, 675 cm^{-1}; ^1H NMR (400 MHz, DMSO-d_6): δ 1.78–1.88 (m, 4H), 2.73–3.30 (m, 10H), 3.51–3.63 (m, 2H), 4.37–4.53 (m, 2H), 7.47–7.56 (m, 3H), 7.68 (d, *J* = 7.0 Hz, 1H), 7.83–7.88 (m, 2H), 8.07 (d, *J* = 8.4 Hz, 1H), 9.06 (d, *J* = 8.7 Hz, 1H), 10.18 (bs, 1H), 12.31 (bs, 1H), 14.63 (bs, 1H) ppm; ^{13}C NMR (100 MHz, DMSO-d_6): δ 20.2, 21.2, 23.5, 25.0, 27.9, 30.6, 49.6, 50.2, 57.3, 110.9, 115.2, 118.7, 125.2, 127.9, 129.5, 130.2, 130.6, 131.3, 132.1, 132.6, 133.3, 138.0, 150.1, 151.4, 159.6 ppm; MS (ESI, MeOH) *m/z*: 419.69 ([M+H]$^+$, 31%), 421.37 ([M+H+2]$^+$, 6%); elemental analysis, calcd. for $C_{25}H_{27}ClN_4$·3 HCl: C, 56.83; H, 5.72; N, 10.60; found: C, 56.66; H, 5.43; N, 10.63.

9-{2-[1-(3-Bromobenzyl)piperidin-4-ylidene]hydrazinyl}-1,2,3,4-tetrahydroacridine trihydrochloride (**H16**): Yellow crystal; 65% yield; mp 200°C (crys. from isopropanol); IR (ATR) ν_{maks}: 2940, 2863, 2661, 2475, 2391, 1634, 1587, 1520, 1471, 1431, 1408, 780, 757, 695 cm^{-1}; ^1H NMR (400 MHz, DMSO-d_6): δ 1.74–1.89 (m, 4H), 2.73–3.31 (m, 10H), 3.50–3.61 (m, 2H), 4.36–4.52 (m, 2H), 7.43 (t, *J* = 7.9 Hz, 1H), 7.52 (ddd, *J* = 8.1/7.3/1.1 Hz, 1H), 7.66 (dd, *J* = 8.1/1.1 Hz, 1H), 7.73 (d, *J* = 7.7 Hz, 1H), 7.85 (ddd, *J* = 8.3/7.1/1.1 Hz, 1H), 7.96–7.99 (m, 1H), 8.07 (d, *J* = 8.0 Hz, 1H), 9.06 (d, *J* = 8.4 Hz, 1H), 10.18 (bs, 1H), 12.30 (bs, 1H), 14.65 (bs, 1H) ppm; ^{13}C NMR (100 MHz, DMSO-d_6): δ 20.2, 21.2, 23.5, 25.0, 27.9, 30.6, 49.6, 50.2, 57.2, 110.8, 115.2, 118.7, 121.9, 125.2, 127.9, 130.6, 130.8, 132.4, 132.6, 134.1, 138.0 (2 C), 150.1, 151.4, 159.6 ppm; MS (ESI, MeOH) *m/z*: 198.43 ([$C_{13}H_{12}N_2$]$^+$, 100%), 463.43 ([M+H]$^+$, 89%), 465.40 ([M+H+2]$^+$, 88%); elemental analysis, calcd. for $C_{25}H_{27}BrN_4$·3 HCl: C, 52.42; H, 5.28; N, 9.78; found: C, 52.82; H, 5.58; N, 9.42.

9-{2-[1-(3-Nitrobenzyl)piperidin-4-ylidene]hydrazinyl}-1,2,3,4-tetrahydroacridine hydrochloride (**H17**): Yellow crystal; 82% yield; mp 238°C (crys. from ethanol); IR (ATR) ν_{maks}: 3083, 2936, 2695,

2655, 1630, 1587, 1520, 1475, 1443, 1405, 1345, 766, 735 cm^{-1}; ^1H NMR (400 MHz, DMSO-d_6): δ 1.80–1.87 (m, 4H), 2.58–2.83 (m, 10H), 2.99–3.07 (m, 2H), 3.69–3.91 (m, 2H), 7.52 (t, *J* = 7.6 Hz, 1H), 7.68 (t, *J* = 7.9 Hz, 1H), 7.81–7.89 (m, 2H), 7.94 (d, *J* = 8.3, 1H), 8.15–8.28 (m, 2H), 9.13 (d, *J* = 8.8 Hz, 1H) ppm; MS (ESI, MeOH) *m/z*: 198.31 ($[C_{13}H_{12}N_2]^+$, 62%), 430.35 ($[M+H]^+$, 100%), 431.40 ($[M+H+1]^+$, 26%); elemental analysis, calcd. for $C_{25}H_{27}N_5O_2$·HCl: C, 64.44; H, 6.06; N, 15.03; found: C, 64.51; H, 6.07; N, 14.80.

9-{2-[1-(3-Cyanobenzyl)piperidin-4-ylidene]hydrazinyl}-1,2,3,4-tetrahydroacridine hydrochloride (**H18**): Yellow crystal; 83% yield; mp 240°C (crys. from ethanol); IR (ATR) ν_{maks}: 2936, 2814, 2688, 2665, 2224, 1629, 1604, 1584, 1519, 1474, 1440, 1402, 780, 766, 688 cm^{-1}; ^1H NMR (400 MHz, DMSO-d_6): δ 1.80–1.88 (m, 4H), 2.59–2.87 (m, 10H), 3.00–3.06 (m, 2H) 3.66–3.88 (m, 2H), 7.53 (t, *J* = 8.4 Hz, 1H), 7.57–7.63 (m, 1H), 7.74–7.89 (m, 4H), 7.93 (d, *J* = 8.4 Hz, 1H), 9.12 (d, *J* = 8.8 Hz, 1H) ppm; MS (ESI, MeOH) *m/z*: 410.45 ($[M+H]^+$, 100%), 411.40 ($[M+H+1]^+$, 32%); elemental analysis, calcd. for $C_{26}H_{27}N_5$·HCl: C, 70.02; H, 6.33; N, 15.70; found: C, 69.71; H, 6.39; N, 15.66.

9-(2-{1-[3-(Trifluoromethyl)benzyl]piperidin-4-ylidene}hydrazinyl)-1,2,3,4-tetrahydroacridine hydrochloride (**H19**): Yellow crystal; 54% yield; mp 223°C (crys. from ethanol); IR (ATR) ν_{maks}: 2945, 2828, 2578, 1630, 1586, 1522, 1475, 1442, 1404, 1325, 1116, 763, 701 cm^{-1}; ^1H NMR (400 MHz, DMSO-d_6): δ 1.79–1.88 (m, 4H), 2.59–2.87 (m, 10H), 2.98–3.06 (m, 2H), 3.71–3.90 (m, 2H), 7.51 (t, *J* = 7.8 Hz, 1H), 7.59–7.76 (m, 4H), 7.83 (t, *J* = 7.6 Hz, 1H), 7.94 (d, *J* = 8.3 Hz, 1H), 9.12 (d, *J* = 8.7 Hz, 1H) ppm; MS (ESI, MeOH) *m/z*: 198.33 ($[C_{13}H_{12}N_2]^+$, 45%), 453.30 ($[M+H]^+$, 100%), 454.33 ($[M+H+1]^+$, 27%); elemental analysis, calcd. for $C_{26}H_{27}F_3N_4$·HCl·H_2O: C, 61.60; H, 5.96; N, 11.05; found: C, 61.87; H, 5.64; N, 10.85.

9-{2-[1-(4-Methylbenzyl)piperidin-4-ylidene]hydrazinyl}-1,2,3,4-tetrahydroacridine trihydrochloride (**H20**): Yellow crystal; 43% yield; mp 201°C (crys. from isopropanol); IR (ATR) ν_{maks}: 2939, 2863, 2692, 2571, 1632, 1586, 1516, 1472, 1408, 802, 758 cm^{-1}; ^1H NMR (400 MHz, DMSO-d_6): δ 1.78–1.90 (m, 4H), 2.34 (s, 3H), 2.73–3.27 (m, 10H), 3.49–3.59 (m, 2H), 4.32–4.43 (m, 2H), 7.27 (d, *J* = 7.9 Hz, 2H), 7.51–7.60 (m, 3H), 7.86 (ddd, *J* = 8.3/6.8/1 Hz, 1H), 8.04 (d, *J* = 8.0 Hz, 1H), 9.07 (d, *J* = 8.8 Hz, 1H), 10.14 (bs, 1H), 12.01 (bs, 1H), 14.50 (bs, 1H ppm; ^{13}C NMR (100 MHz, DMSO-d_6): δ 20.7, 21.3, 21.7, 24.0, 25.5, 28.4, 31.1, 49.8, 50.4, 58.4, 111.3, 115.7, 119.2, 125.6, 127.2, 128.4, 129.7 (2 C), 131.9 (2 C), 133.0, 138.5, 139.4, 150.6, 151.8, 160.2 ppm; MS (ESI, MeOH) *m/z*: 198.32 ($[C_{13}H_{12}N_2]^+$, 55%), 398.37 ($[M-H]^+$, 12%), 399.39 ($[M+H+]^+$, 100%) 400.31 ($[M+H+1]^+$, 10%); elemental analysis, calcd. for $C_{26}H_{30}N_4$·3 HCl: C, 61.48; H, 6.55; N, 11.03; found: C, 61.70; H, 6.24; N, 10.93.

9-{2-[1-(4-Fluorobenzyl)piperidin-4-ylidene]hydrazinyl}-1,2,3,4-tetrahydroacridine trihydrochloride (**H21**): Yellow crystal; 27% yield; mp 201°C (crys. from isopropanol); IR (ATR) ν_{maks}: 3059, 2942, 2688, 2579, 1632, 1587, 1511, 1459, 1407, 759, 677 cm^{-1}; ^1H NMR (400 MHz, DMSO-d_6): δ 1.77–1.89 (m, 4H), 2.73–3.29 (m, 10H), 3.50–3.61 (m, 2H), 4.34–4.50 (m, 2H), 7.31 (t, *J* = 8.9 Hz, 2H), 7.53 (t, *J* = 7.9 Hz, 1H), 7.77 (dd, *J* = 8.4/5.6 Hz, 1H), 7.85 (t, *J* = 7.7 Hz, 1H), 8.06 (d, *J* = 8.5 Hz, 1H), 9.06 (d, *J* = 8.8 Hz, 1H), 10.18 (bs, 1H), 12.21 (bs, 1H), 14.62 (bs, 1H) ppm; ^{13}C NMR (100 MHz, DMSO-d_6): δ 20.3, 21.2, 23.5, 25.0, 27.9, 30.7, 49.4, 50.0, 57.2, 110.9, 115.2, 115.6, 115.8, 118.7, 125.2, 126.1, 127.9, 132.6, 133.9, 138.0, 150.1, 151.4, 159.7, 161.5, 163.9 ppm; MS (ESI, MeOH) *m/z*: 222.94 ($[C_{14}H_{13}N_3]^+$, 100%), 403.73 ($[M+H]^+$, 97%), 404.70 ($[M+H+1]^+$, 14%); elemental analysis, calcd. for $C_{25}H_{27}FN_4$·3 HCl: C, 58.66; H, 5.91; N, 10.95; found: C, 58.44; H, 5.91; N, 10.93.

9-{2-[1-(4-Chlorobenzyl)piperidin-4-ylidene]hydrazinyl}-1,2,3,4-tetrahydroacridine trihydrochloride (**H22**): Yellow crystal; 13% yield; mp 220°C (crys. from isopropanol); IR (ATR) ν_{maks}: 2942, 2783, 2695, 2531, 2423, 1633, 1586, 1516, 1474, 1408, 804, 756, 675 cm^{-1}; ^1H NMR (400 MHz, DMSO-d_6): δ 1.75–1.90 (m, 4H), 2.73–3.29 (m, 10H), 3.49–3.61 (m, 2H), 4.35–4.50 (m, 2H), 7.50–7.57 (m, 3H), 7.74 (d, *J* = 8.4 Hz, 2H), 7.86 (ddd, *J* = 8.2/6.8/0.8 Hz, 1H), 8.06 (d, *J* = 8.3 Hz, 1H), 9.05 (d, *J* = 8.7 Hz, 1H), 10.17 (bs, 1H), 12.26 (bs, 1H), 14.59 (bs, 1H) ppm; ^{13}C NMR (100 MHz, DMSO-d_6): δ 20.3, 21.2, 23.5, 25.1, 28.0, 30.6, 49.5, 50.1, 57.3, 110.9, 115.2, 118.7, 125.2, 127.9, 128.7, 128.8 (2 C), 132.7, 133.4 (2 C), 134.4, 138.0, 150.2, 151.4, 159.7 ppm; MS (ESI, MeOH) *m/z*: 419.66 ($[M+H]^+$, 29%), 421.60 ($[M+H+2]^+$, 9%); elemental analysis, calcd. for $C_{25}H_{27}ClN_4$·3 HCl: C, 56.83; H, 5.72; N, 10.60; found: C, 56.90; H, 5.59; N, 10.37.

9-{2-[1-(4-Bromobenzyl)piperidin-4-ylidene]hydrazinyl}-1,2,3,4-tetrahydroacridine trihydrochloride (**H23**): Yellow crystal; 18% yield; mp 208°C (crys. from isopropanol); IR (ATR) ν_{maks}: 2943, 2692, 2576, 1633, 1587, 1517, 1491, 1473, 1409, 756, 677 cm^{-1}; ^1H NMR (400 MHz, DMSO-d_6): δ 1.79–1.91 (m, 4H), 2.76–3.24 (m, 10H), 3.50–3.62 (m, 2H), 4.31–4.48 (m, 2H), 7.55 (t, *J* = 7.8 Hz, 1H), 7.61–7.71 (m, 4H), 7.87 (t, *J* = 7.7 Hz, 1H), 8.02 (d, *J* = 8.5 Hz, 1H), 9.08 (d, *J* = 9.1 Hz, 1H), 10.12 (bs, 1H), 12.13 (bs, 1H), 14.36 (bs, 1H) ppm; ^{13}C NMR (100 MHz, DMSO-d_6): δ 20.3, 21.2, 23.5, 25.1, 28.0, 30.7, 49.5, 50.1, 57.3, 110.9, 115.2, 118.7, 123.2, 125.2, 128.0, 129.1, 131.7 (2 C), 132.7, 133.7 (2 C), 138.0, 150.2, 151.4, 159.7 ppm; MS (ESI, MeOH) *m/z*: 198.35 ($[C_{13}H_{12}N_2]^+$, 100%), 463.32 ($[M+H]^+$, 16%), 465.30 ($[M+H+2]^+$, 16%); elemental analysis, calcd. for $C_{25}H_{27}BrN_4$·3 HCl·0.25 H_2O: C, 52.01; H, 5.33; N, 9.70; found: C, 51.70; H, 5.41; N, 9.55.

9-{2-[1-(4-Nitrobenzyl)piperidin-4-ylidene]hydrazinyl}-1,2,3,4-tetrahydroacridine hydrochloride (**H24**): Yellow crystal; 22% yield; mp 218°C (crys. from ethanol); IR (ATR) ν_{maks}: 2329, 2849, 2479, 2412, 1632, 1585, 1516, 1470, 1437, 1405, 1344, 856, 763, 690 cm^{-1}; ^1H NMR (400 MHz, DMSO-d_6): δ 1.89–1.99 (m, 4H), 2.79–3.09 (m, 8H), 3.30–3.51 (m, 2H), 3.64–3.79 (m, 2H), 4.63 (s, 2H), 7.55 (t, *J* = 7.9 Hz, 1H), 7.82 (d, *J* = 8.4 Hz, 1H), 7.89 (t, *J* = 7.7 Hz, 1H), 7.94 (d, *J* = 8.4 Hz, 2H), 8.37 (d, *J* = 8.3 Hz, 2H), 9.23 (d, *J* = 9.0 Hz, 1H) ppm; MS (ESI, MeOH) *m/z*: 430.72 ($[M+H]^+$, 100%), 431.70 ($[M+H+1]^+$, 30%); elemental analysis, calcd. for $C_{25}H_{27}N_5O_2$·3HCl: 55.72; H, 5.61; N, 13.00; found: C, 55.87; H, 5.40; N, 13.02.

9-{2-[1-(4-Cyanobenzyl)piperidin-4-ylidene]hydrazinyl}-1,2,3,4-tetrahydroacridine hydrochloride (**H25**): Yellow crystal; 20% yield; mp 225°C (crys. from ethanol); IR (ATR) ν_{maks}: 3048, 2940, 2792, 2692,2640, 2440, 2313, 2225, 1629, 1585, 1519, 1472, 1403, 761, 679 cm^{-1}; ^1H NMR (400 MHz, DMSO-d_6): δ 1.79–1.87 (m, 4H), 2.57–2.58 (m, 10H), 2.29–3.05 (m, 2H), 3.70–3.79 (m, 2H), 7.49 (t, *J* = 7.8 Hz, 1H), 7.56–7.64 (m, 2H), 7.78–7.86(m, 3H), 7.98 (d, *J* = 9.3 Hz,

1H), 9.10 (d, J = 8.7 Hz, 1H) ppm; MS (ESI, MeOH) *m/z*: 198.32 ($[C_{13}H_{12}N_2]^+$, 82%), 410.37 ($[M+H]^+$, 100%), 411.40 ($[M+H+1]^+$, 23%); elemental analysis, calcd. for $C_{26}H_{27}N_5$·HCl·0.5 H_2O·0.5 C_3H_7OH: C, 68.10; H, 6.86; N, 14.44; found: C, 67.82; H, 6.58; N, 14.30.

9-(2-{1-[4-(Trifluoromethyl)benzyl]piperidin-4-ylidene}hydrazinyl)-1,2,3,4-tetrahydroacridine trihydrochloride (**H26**): Yellow crystal; 15% yield; mp 225°C (crys. from ethanol); IR (ATR) ν_{maks}: 2937, 2765, 2692, 2654, 2486, 2388, 1632, 1585, 1519, 1473, 1408, 1324, 1161, 1115, 760, 677 cm^{-1}; ^1H NMR (400 MHz, DMSO-d_6): δ 1.80–1.90 (m, 4H), 2.71–3.27 (m, 10H), 3.52–3.64 (m, 2H), 4.31–4.61 (m, 2H), 7.56 (t, J = 8.3 Hz, 1H), 7.55–7.97 (m, 5H), 8.01 (d, J = 8.6 Hz, 1H), 9.09 (d, J = 8.6 Hz, 1H), 10.13 (bs, 1H), 12.28 (bs, 1H), 14.33 (bs, 1H) ppm; MS (ESI, MeOH) *m/z*: 198.31 ($[C_{13}H_{12}N_2]^+$, 82%), 453.35 ($[M+H]^+$, 100%), 454.32 ($[M+H+1]^+$, 24%); elemental analysis, calcd. for $C_{26}H_{27}F_3N_4$·3HCl: C, 55.58; H, 5.38; N, 9.97; found: C, 55.27; H, 5.02; N, 9.90.

9-{2-[1-(2,6-Difluorobenzyl)piperidin-4-ylidene]hydrazinyl}-1,2,3,4-tetrahydroacridine trihydrochloride (**H27**): Yellow crystal; 81% yield; mp 250°C (crys. from isopropanol); IR (ATR) ν_{maks}: 2937, 2695, 2657, 2554, 2510,1627, 1585, 1521, 1471, 1430, 1404, 895, 763, 676 cm^{-1}; ^1H NMR (400 MHz, DMSO-d_6): δ 1.76–1.88 (m, 4H), 2.74–3.39 (m, 10H), 3.59–3.70 (m, 2H), 4.42 (s, 2H), 7.26 (t, J = 8.2 Hz, 2H), 7.53 (t, J = 7.9 Hz,1H), 7.64 (ddd, J = 8.2/6.9/1.3 Hz, 1H), 7.85 (t, J = 7.4 Hz, 1H), 8.09 (d, J = 8.4 Hz, 1H), 9.08 (d, J = 8.7 Hz, 1H), 10.17 (bs, 1H), 12.21 (bs, 1H), 14.70 (bs, 1H) ppm; ^{13}C NMR (100 MHz, DMSO-d_6): δ 20.3, 21.2, 23.5, 25.5, 27.9, 49.7, 50.7, 62.0, 110.8, 112.0, 112.2 (2 C), 115.2, 118.7, 125.2, 128.1, 132.6 (2 C), 138.1, 150.1, 151.4, 160.3, 162.9 (2 C) ppm; MS (ESI, MeOH) *m/z*: 421.46 ($[M+H]^+$, 100%), 422.40 ($[M+H+1]^+$, 32%); elemental analysis, calcd. for $C_{25}H_{26}F_2N_4$·3 HCl·0.4 C_3H_7OH: C, 56.81; H, 5.86; N, 10.11; found: C, 56.75; H, 6.23; N, 9.90.

9-{2-[1-(2,6-Dichlorobenzyl)piperidin-4-ylidene]hydrazinyl}-1,2,3,4-tetrahydroacridine trihydrochloride (**H28**): Yellow crystal; 70% yield; mp 190°C (crys. from isopropanol); IR (ATR) ν_{maks}: 2958, 2858, 2545, 2454, 1631, 1583, 1519, 1474, 1437, 1411, 792, 762, 702 cm^{-1}; ^1H NMR (400 MHz, DMSO-d_6): δ 1.77–1.88 (m, 4H), 2.74–3.34 (m, 10H), 3.55–3.69 (m, 2H), 4.62 (s, 2H), 7.51–7.57 (m, 2H), 7.63 (d, J = 8.0 Hz, 2H), 7.86 (t, J = 7.7 Hz, 1H), 8.10 (d, J = 8.4 Hz, 1H), 9.10 (d, J = 8.8 Hz, 1H), 10.24 (bs, 1H), 11.42 (bs, 1H), 14.72 (bs, 1H) ppm; ^{13}C NMR (100 MHz, DMSO-d_6): δ 20.3, 21.3, 23.6, 25.3, 25.5, 27.9, 51.3, 52.4, 54.5, 110.9, 115.2, 118.7, 125.2, 128.0, 129.2 (3 C), 132.6 (2 C), 137.1 (2 C), 138.1, 150.1, 151.4, 159.5 ppm; MS (ESI, MeOH) *m/z*: 198.31 ($[C_{13}H_{12}N_2]^+$, 100%), 453.35 ($[M+H]^+$, 22%), 455.33 ($[M+H+2]^+$, 14%), 457.33 ($[M+H+4]^+$, 4%); elemental analysis, calcd. for $C_{25}H_{26}Cl_2N_4$·3 HCl·0.75 H_2O: C, 52.10; H, 5.33; N, 9.72; found: C, 52.30; H, 5.45; N, 9.43.

4.2 | Pharmacological/biological assays

4.2.1 | ChE inhibition

Inhibition of eeAChE and eqBChE activities

AChE (E.C. 3.1.1.7., Type VI-S, from electric eel) and BChE (E.C. 3.1.1.8, from equine serum) were purchased from Sigma-Aldrich. 5,5′-Dithiobis(2-nitrobenzoic acid) (DTNB, Ellman's reagent) acetylthiocholine iodide (ATC), and butyrylthiocholine iodide (BTC) were obtained from Fluka. Buffer salts (potassium dihydrogen phosphate, potassium hydroxide) and sodium hydrogen carbonate were purchased from Merck. Spectrophotometric measurements were performed on a Shimadzu 160-A UV-Vis spectrophotometer.

The inhibitory effects of the final compounds on AChE and BChE were evaluated using a slightly modified Ellman's method.[26,31] Tacrine was used as a reference compound. Before use, all solutions were adjusted to 20°C. Enzyme solution (50 µL) and inhibitor solution (50 µL) were added into cuvettes containing phosphate buffer (1.5 mL; 0.1 M, pH 8.0). After 5 min incubation, aliquots of DTNB solution (50 µL) and substrate, that is, ATC or BTC (10 µL), were added to start the reaction. After rapid and immediate mixing, absorption at 412 nm was measured. The assay was carried out in the absence and presence of an inhibitor. The blank solutions were prepared in parallel and contained 1.5 mL buffer, 100 µL water, 50 µL DTNB, and 10 µL substrate. The enzyme activity was determined in the presence of at least five different concentrations of inhibitor, generally between 10^{-3} and 10^{-9} M, to obtain inhibition of AChE or BChE activity between 0% and 100%. Each concentration was assayed in triplicate.

Inhibition of hAChE and hBChE activities

Initial rate assays were performed at 37°C using a Jasco V-530 double-beam Spectrophotometer (Jasco Europe). The rate of increase in the absorbance at 412 nm was followed for 3 min. AChE stock solution was prepared by dissolving human recombinant AChE (E.C.3.1.1.7) lyophilized powder (Sigma) in 0.1 M phosphate buffer (pH = 8.0) containing Triton X-100 0.1%. The stock solution of BChE from human serum was prepared by dissolving the lyophilized powder (Sigma) in an aqueous solution of 0.1% gelatin. Stock solutions of inhibitors (2 mM) were prepared in methanol. Five increasing concentrations of inhibitor were used, able to give an inhibition of the enzymatic activity in the range of 20%–80%. The assay solution consisted of a 0.1 M phosphate buffer pH 8.0, with the addition of 340 µM DTNB, 0.02 unit/mL of human recombinant AChE or *h*BChE, and 550 µM of substrate (ATC or BTC). A volume of 50 µL aliquots of increasing concentrations of the tested compound were added to the assay solution and preincubated for 20 min at 37°C prior to the addition of the substrate. In parallel, blank solutions containing all components except the enzyme were prepared to account for the nonenzymatic hydrolysis of the substrate in the assay buffer. The reaction rates obtained in the absence and presence of the inhibitor were compared and the percent inhibition due to the presence of tested inhibitor at increasing concentration was calculated. Each concentration was analyzed in duplicate, and IC_{50} values were determined graphically from log concentration–inhibition curves (GraphPad Prism 4.03 software, GraphPad Software Inc.).[31]

Kinetic characterization of AChE and BChE inhibition

Compounds **H4** and **H15** were selected to investigate the mechanism of action of *h*AChE, *h*BChE, and *ee*AChE, *eq*BChE inhibition,

respectively. Investigations were carried out, adapting Ellman's method.[31] Three different concentrations of **H4**, namely, 0.25, 0.5, 1 μM, and **H15**, namely 0.05, 0.1, and 0.2 μM, were selected to assess kinetics of AChE inhibition while inhibitor concentrations of 0.025, 0.05, 0.1 μM for **H4** and 0.015, 0.03, 0.06 μM for **H15** were used for investigations on BChE. Concentrations of substrate, either ATC or BTC, ranged from 0.11 to 0.68 mM (in detail: 0.11, 0.17, 0.23, 0.34, 0.45, 0.56, and 0.68 mM). The assay was performed in triplicate. The inhibition mode was determined by building Lineweaver–Burk plots, that is, reciprocal plots of 1/*V* versus 1/[S], by SigmaPlot 12.5.

4.2.2 | Cell viability assay

SH-SY5Y cells 5×10^3 cells/well were incubated for 24 h. After 24 h, the cells were treated with compounds at indicated concentrations (0.1, 1, and 10 μM) for 2 h. Cells were treated with 250 μM of H_2O_2 in sterile PBS (with Ca^{2+} and Mg^{2+}) for 1 h. After 1 h, the H_2O_2 solution was replaced with a warm medium and incubated for 17 h. After the 18 h exposure, the cell viability was determined using the 2-(4-iodophenyl)-3-(4-nitrophenyl)-5-(2,4-disulfophenyl)-2H-tetrazolium (WST-1) assay kit (Takara Bio Inc.). Briefly, following exposures, 10 μL Premix WST-1 was added to each well, and plates were incubated for 2 h at 37°C in a 5% CO_2 humidified incubator. Then the absorbance was measured at 440 nm using a microplate reader (VersaMax, Molecular Devices). Percent survival was plotted relative to vehicle control cells, which were normalized to 100% survival. At the same time, all compounds, alone, were evaluated for possible cytotoxicity.[42] To screen hepatotoxicity, HepG2 human hepatocellular carcinoma cells were exposed to the test compounds (0.1, 1, and 10 μM) for 24 h. Cell viability was measured by using WST-1 as described above.

4.2.3 | BBB permeability assay

Human cerebral microvascular endothelial cells (HBEC-5i, ATCC, CRL-3245) were cultivated with Dulbecco's Modified Eagle Medium/Nutrient Mixture F12 (DMEM/F12), supplemented with 40 μg/mL endothelial growth supplement (ECGs, E2759, Sigma-Aldrich) and 10% fetal bovine serum (FB, A0500-3010, Cegrogen). To obtain the BBB model, PET membrane transwell inserts (Thincert, 662610, Greiner Bio-One) were used. Insert membrane was coated with sterile 0.1% porcine gelatin (G2500, Sigma-Aldrich) solution before the cell seeding. HBEC-5i cells were trypsinized, seeded at 1×10^6 cells/cm^2 on the inserts, and cultivated for 24 h in a humidified cell culture incubator (37°C and 5% CO_2). Lucifer Yellow CH dipotassium salt (LY, L0144, Sigma-Aldrich) molecule was passed through the model to control the permeability of the models. The permeability was calculated as follows:

$$P\left(\frac{\text{cm}}{\text{s}}\right) = \frac{V\,(\text{cm}^3)}{A\,(\text{cm}^2) \times [C]_{\text{apical}}\left(\frac{\text{g}}{\text{mL}}\right)} \times \frac{\Delta [C]_{\text{basolateral}}\left(\frac{\text{g}}{\text{mL}}\right)}{\Delta t\,(\text{s})},$$

where *P* is the permeability value, *V* is the volume of the media in the basolateral part, *A* is the cross-sectional surface area of the hydrogel, and [*C*] is the concentration of the molecule.

It is suggested that the LY permeability value should be $<2 \times 10^{-6}$ cm/s to show that the tight junctions between endothelial cells are suitable for modeling the BBB. The permeability value of the LY passed through the models for 60 min was found to be 5×10^{-6} cm/s. A longer period of cell cultivation is required to obtain lower permeability values, but since the cells are sensitive and detach from the PET membrane surface after the 2nd day, it was decided that the LY permeability value obtained for the model was suitable for performing the test.

Compounds **H6** (0.1 mM), **H15** (0.1 mM), **H20** (0.1 mM), and tacrine HCl (0.1 mM and 0.5 mM) were prepared in Ringer's HEPES solution, and **H6**, **H15**, **H20** concentrations were measured at 248 nm, and the tacrine HCl concentration was measured at 238 nm. Calibration graphs were obtained. After calibration, all compounds were passed through the model for 60 min (three replicates), and the permeability values were calculated according to the formula above.[43]

4.2.4 | Statistical analysis

All quantitative data values of BBB permeability are represented as means ± standard deviation of experiments made with three replicates ($n = 3$). Statistical analyses were performed using the parametric two-way analysis of variance (ANOVA) test. Multiple comparisons were analyzed using Tukey's post-hoc method. Statistical significance was described in all statistical analyses accordingly ($p < 0.05$, $p < 0.01$, $p < 0.001$, and $p < 0.0001$). All data were statistically analyzed using the GraphPad Prism 7 Statistic Program.

4.3 | Molecular modeling

The Schrödinger Suite 2018-1[44] and OPLS_2005 force field[45] were considered for all molecular modeling tasks. The theoretical pharmacokinetic properties of all derivatives were predicted using the QikProp tool. The *h*AChE and *h*BChE enzyme three-dimensional models were obtained from the Protein Data Bank (PDB)[37] crystallographic structures 4EY7[46] and 5NN0,[47] respectively. Both PDB entries used in this study were chosen not only taking into account the absence of mutation and the presence of a reversible ligand but also the resolution, R-free value, and the diffraction-component precision index (DPI)[48,49], a global criterion that assesses both model and data quality. Before computing the grid for docking simulation, *h*ChE structures were adjusted employing the Protein Preparation Wizard.[50] The workflow includes the assignment of correct atom bond orders, the addition of hydrogen, the optimization of hydrogen bonds, the determination of the most favorable ligand protonation state, and the minimization of the protein. Then, target binding sites were defined by means of a regular grid box of about

64,000 Å^3 centered on the catalytic serine residues. All docking simulations were computed using Glide[51] (ligand flexible algorithm at standard-precision (SP) level. MD investigations were performed using Desmond software.[52] The SPC explicit solvent model was applied for generating solvated systems. The overall electrostatic net charge was neutralized including Na^+ ions into the *h*AChE systems and Cl^- ions into the *h*BChE ones. The default Desmond protocol was applied for equilibrating solvated systems. The production run of MD simulations was executed at 300 K, up to 250 ns, with an integration time step equal to 2 fs. MD frames were sampled at regular time intervals equal to 250 ps, collecting 1000 frames for each simulation.

ACKNOWLEDGMENTS

The authors thank the Pharmaceutical Sciences Research Centre (FABAL) at Ege University Faculty of Pharmacy for spectral analyses of the compounds. The authors also thank the COST action CA15135 for support. This work was supported by Research Grants from Ege University (Project Number: 16ECZ023).

CONFLICTS OF INTEREST STATEMENT

The authors declare no conflicts of interest.

DATA AVAILABILITY STATEMENT

Data that support the findings of this study are available in the supplementary material of this article.

ORCID

Vildan Alptüzün http://orcid.org/0000-0002-1477-4440

REFERENCES

[1] P. Scheltens, B. De Strooper, M. Kivipelto, H. Holstege, G. Chételat, C. E. Teunissen, J. Cummings, W. M. van der Flier, *Lancet* **2021**, *397*, 1577. https://doi.org/10.1016/S0140-6736(20)32205-4

[2] C. Patterson, World Alzheimer Report 2018 - The state of the art of dementia research: New frontiers, Alzheimer's Dis. Int. (**2018**). https://www.alz.co.uk/research/WorldAlzheimerReport2018.pdf

[3] J. Cummings, G. Lee, P. Nahed, M. E. Z. N. Kambar, K. Zhong, J. Fonseca, K. Taghva, *Alzheimer's Dement. Transl. Res. Clin. Interv.* **2022**, *8*, 12295. https://doi.org/10.1002/trc2.12295

[4] J. Cummings, G. Lee, A. Ritter, K. Zhong, *Alzheimer's Dement. Transl. Res. Clin. Interv.* **2018**, *4*, 195. https://doi.org/10.1016/j.trci.2018.03.009

[5] S. Gunes, Y. Aizawa, T. Sugashi, M. Sugimoto, P. P. Rodrigues, *Int. J. Mol. Sci.* **2022**, *23*, 4962. https://doi.org/10.3390/ijms23094962

[6] J. Cummings, *Mol. Neurodegener.* **2021**, *16*, 2. https://doi.org/10.1186/s13024-021-00424-9

[7] J. Cummings, G. Lee, K. Zhong, J. Fonseca, K. Taghva, *Alzheimer's Dement. Transl. Res. Clin. Interv.* **2021**, *7*, 12179. https://doi.org/10.1002/trc2.12179

[8] E. Scarpini, P. Schelterns, H. Feldman, *Lancet Neurol.* **2003**, *2*, 539. https://doi.org/10.1016/S1474-4422(03)00502-7

[9] A. Cavalli, M. L. Bolognesi, A. Minarini, M. Rosini, V. Tumiatti, M. Recanatini, C. Melchiorre, *J. Med. Chem.* **2008**, *51*, 347. https://doi.org/10.1021/jm7009364

[10] J., Lalut, C., Rochais, P., Dallemagne, *An Evol. Concept Med. Chem.* **2017**, 477. https://doi.org/10.1002/9783527674381.ch16

[11] S. M. Hoy, *Drugs*, 83, **2023**, pp. 359. https://doi.org/10.1007/s40265-023-01851-2

[12] K. P. Kepp, *Chem. Rev.* **2012**, *112*, 5193. https://doi.org/10.1021/cr300009x

[13] F. J. Pérez-Areales, M. Garrido, E. Aso, M. Bartolini, A. De Simone, A. Espargaró, T. Ginex, R. Sabate, B. Pérez, V. Andrisano, D. Puigoriol-Illamola, M. Pallàs, F. J. Luque, M. I. Loza, J. Brea, I. Ferrer, F. Ciruela, A. Messeguer, D. Muñoz-Torrero, *J. Med. Chem.* **2020**, *63*, 9360. https://doi.org/10.1021/acs.jmedchem.0c00528

[14] N. C. Inestrosa, R. Alarcón, *J. Physiol. Paris* **1998**, *92*, 341. https://doi.org/10.1016/S0928-4257(99)80002-3

[15] N. H. Greig, T. Utsuki, Q.-S. Yu, X. Zhu, H. W. Holloway, T. Perry, B. Lee, D. K. Ingram, D. K. Lahiri, *Curr. Med. Res. Opin.* **2001**, *17*, 159. https://doi.org/10.1185/0300799039117057

[16] A. L. Guillozet, M.-M. Mesulam, J. F. Smiley, D. C. Mash, *Ann. Neurol.* **1997**, *42*, 909. https://doi.org/10.1002/ana.410420613

[17] M. Decker, *Mini-Rev. Med. Chem.* **2007**, *7*, 221. https://doi.org/10.2174/138955707780059817

[18] *Design of Hybrid Molecules for Drug Development* (M. Decker ed.), Elsevier, **2017**.

[19] L. Savini, A. Gaeta, C. Fattorusso, B. Catalanotti, G. Campiani, L. Chiasserini, C. Pellerano, E. Novellino, D. McKissic, A. Saxena, *J. Med. Chem.* **2003**, *46*, 1. https://doi.org/10.1021/jm0255668

[20] L. Piazzi, A. Rampa, A. Bisi, S. Gobbi, F. Belluti, A. Cavalli, M. Bartolini, V. Andrisano, P. Valenti, M. Recanatini, *J. Med. Chem.* **2003**, *46*, 2279. https://doi.org/10.1021/jm0340602

[21] M. Bolognesi, A. Minarini, M. Rosini, V. Tumiatti, C. Melchiorre, *Mini-Rev. Med. Chem.* **2008**, *8*, 960. https://doi.org/10.2174/138955708785740652

[22] H. Lin, Q. Li, K. Gu, J. Zhu, X. Jiang, Y. Chen, H. Sun, *Curr. Top. Med. Chem.* **2017**, *17*, 3000. https://doi.org/10.2174/1568026617666170717114944

[23] M. Recanatini, A. Cavalli, F. Belluti, L. Piazzi, A. Rampa, A. Bisi, S. Gobbi, P. Valenti, V. Andrisano, M. Bartolini, V. Cavrini, *J. Med. Chem.* **2000**, *43*, 2007. https://doi.org/10.1021/jm990971t

[24] Q. Li, S. He, Y. Chen, F. Feng, W. Qu, H. Sun, *Eur. J. Med. Chem.* **2018**, *158*, 463. https://doi.org/10.1016/j.ejmech.2018.09.031

[25] M. Bartolini, C. Bertucci, V. Cavrini, V. Andrisano, *Biochem. Pharmacol.* **2003**, *65*, 407. https://doi.org/10.1016/S0006-2952(02)01514-9

[26] S. Parlar, G. Bayraktar, A. H. Tarikogullari, V. Alptüzün, E. Erciyas, *Chem. Pharm. Bull.* **2016**, *64*, 1281. https://doi.org/10.1248/cpb.c16-00221

[27] M. Prinz, S. Parlar, G. Bayraktar, V. Alptüzün, E. Erciyas, A. Fallarero, D. Karlsson, P. Vuorela, M. Burek, C. Förster, E. Turunc, G. Armagan, A. Yalcin, C. Schiller, K. Leuner, M. Krug, C. A. Sotriffer, U. Holzgrabe, *Eur. J. Pharm. Sci.* **2013**, *49*, 603. https://doi.org/10.1016/j.ejps.2013.04.024

[28] S. Rollas, S. Küçükgüzel, *Molecules* **2007**, *12*, 1910. https://doi.org/10.3390/12081910

[29] G. A. K. Teponnou, J. Joubert, S. F. Malan, *Open Med. Chem. J.* **2017**, *11*, 24. https://doi.org/10.2174/1874104501711010024

[30] E. Große Maestrup, C. Wiese, D. Schepmann, A. Hiller, S. Fischer, M. Scheunemann, P. Brust, B. Wünsch, *Bioorg. Med. Chem.* **2009**, *17*, 3630. https://doi.org/10.1016/j.bmc.2009.03.060

[31] G. L. Ellman, K. D. Courtney, V. Andres, R. M. Feather-Stone, *Biochem. Pharmacol.* **1961**, *7*, 88.

[32] M. Hoffmann, C. Stiller, E. Endres, M. Scheiner, S. Gunesch, C. Sotriffer, T. Maurice, M. Decker, *J. Med. Chem.* **2019**, *62*, 9116. https://doi.org/10.1021/acs.jmedchem.9b01012

[33] D. Shao, C. Zou, C. Luo, X. Tang, Y. Li, *Bioorg. Med. Chem. Lett.* **2004**, *14*, 4639. https://doi.org/10.1016/j.bmcl.2004.07.005

[34] M. Girek, P. Szymański, *Chem. Pap.* **2019**, *73*, 269. https://doi.org/10.1007/s11696-018-0590-8

[35] L. Ismaili, B. Refouvelet, M. Benchekroun, S. Brogi, M. Brindisi, S. Gemma, G. Campiani, S. Filipic, D. Agbaba, G. Esteban, M. Unzeta, K. Nikolic, S. Butini, J. Marco-Contelles, *Prog. Neurobiol.* **2017**, *151*, 4. https://doi.org/10.1016/j.pneurobio.2015.12.003

[36] K. V. Dileep, K. Ihara, C. Mishima-Tsumagari, M. Kukimoto-Niino, M. Yonemochi, K. Hanada, M. Shirouzu, K. Y. J. Zhang, *Int. J. Biol. Macromol.* **2022**, *210*, 172. https://doi.org/10.1016/j.ijbiomac.2022.05.009
[37] H. M. Berman, *Nucleic Acids Res.* **2000**, *28*, 235. https://doi.org/10.1093/nar/28.1.235
[38] F. Nachon, E. Carletti, C. Ronco, M. Trovaslet, Y. Nicolet, L. Jean, P.-Y. Renard, *Biochem. J.* **2013**, *453*, 393. https://doi.org/10.1042/BJ20130013
[39] P. Szymanski, A. Karpiński, E. Mikiciuk-Olasik, *Eur. J. Med. Chem.* **2011**, *46*, 3250. https://doi.org/10.1016/j.ejmech.2011.04.038
[40] J. Bielavsky, *Chem. Commun.* **1977**, *42*, 2802.
[41] H. Fakhraian, M. B. P. Riseh, *Org. Prep. Proced. Int.* **2008**, *40*, 307. https://doi.org/10.1080/00304940809458092
[42] A. Minarini, A. Milelli, V. Tumiatti, M. Rosini, E. Simoni, M. L. Bolognesi, V. Andrisano, M. Bartolini, E. Motori, C. Angeloni, S. Hrelia, *Neuropharmacology* **2012**, *62*, 997. https://doi.org/10.1016/j.neuropharm.2011.10.007
[43] E. Bayir, M. M. Celtikoglu, A. Sendemir, *Int. J. Biol. Macromol.* **2019**, *126*, 1002. https://doi.org/10.1016/j.ijbiomac.2018.12.257
[44] L. L. C. Schrödinger, L. L. C. Schrödinger, (**2018**).
[45] W. L. Jorgensen, D. S. Maxwell, J. Tirado-Rives, *J. Am. Chem. Soc.* **1996**, *118*, 11225. https://doi.org/10.1021/ja9621760
[46] J. Cheung, M. J. Rudolph, F. Burshteyn, M. S. Cassidy, E. N. Gary, J. Love, M. C. Franklin, J. J. Height, *J. Med. Chem.* **2012**, *55*, 10282. https://doi.org/10.1021/jm300871x
[47] U. Košak, B. Brus, D. Knez, S. Žakelj, J. Trontelj, A. Pišlar, R. Šink, M. Jukič, M. Živin, A. Podkowa, F. Nachon, X. Brazzolotto, J. Stojan, J. Kos, N. Coquelle, K. Sałat, J.-P. Colletier, S. Gobec, *J. Med. Chem.* **2018**, *61*, 119. https://doi.org/10.1021/acs.jmedchem.7b01086
[48] G. L. Warren, T. D. Do, B. P. Kelley, A. Nicholls, S. D. Warren, *Drug Discov. Today* **2012**, *17*, 1270. https://doi.org/10.1016/j.drudis.2012.06.011
[49] D. M. Blow, *Acta Crystallogr. D. Biol. Crystallogr.* **2002**, *58*, 792. https://doi.org/10.1107/S0907444902003931
[50] L. L. C. Schrödinger, Protein Preparation Wizard, (**2018**).
[51] S. LLC, Glide, (**2018**).
[52] D.E.S. Research, Desmond Molecular Dynamics System, (**2018**) 2018.

SUPPORTING INFORMATION

Additional supporting information can be found online in the Supporting Information section at the end of this article.

How to cite this article: G. Bayraktar, M. Bartolini, M. L. Bolognesi, M. A. Erdoğan, G. Armağan, E. Bayır, A. Şendemir, D. Bagetta, S. Alcaro, V. Alptüzün, *Arch. Pharm.* **2024**;*357*:e2300575. https://doi.org/10.1002/ardp.202300575